# A Three-dimensional Simulation of the Hudson-Raritan Estuary

## Part I: Description of the Model and Model Simulations

by



Li-Yauw Oey

George L. Mellor

Geophysical Fluid Dynamics Program

James Forrestal Campus

Princeton University

Princeton, NJ 08542

Richard I. Hires

Department of Civil & Ocean Engineering

Stevens Institute of Technology

Hoboken, NJ 07030



May, 1984

This research was sponsored by the New Jersey Sea Grant program under a grant from the Office of Sea Grant of NOAA, Grant no. NA81 AA-D00065, Project no. R/E-3. Additional funding was provided under Grant no. NA 80 RAD 00033 from the Northeast Office of the Office of Marine Pollution Assessment of NOAA. LYO was supported in part by the Visiting Scientist Program of Princeton University/NOAA, Grant 04-7-022-44017.

## ABSTRACT

A time-dependent, three dimensional, finite-difference simulation of the Hudson-Raritan estuary is presented. The calculation covers July through September, 1980 and includes real tide and wind forcing and also time-dependent river and sewage discharges. Turbulence mixing coefficients in the estuary are calculated according to second moment, turbulence closure sub-model. Salinity contours show formation of complex pattern of eddies produced by the interaction of the unsteady, three dimensional velocity field with coastline and bottom bathymetries. These eddies are advected and subsequently mixed throughout the water column and are important physical elements in shear dispersion processes in the estuary.

The effect of wind on the vertical salinity structure is significant in shallow regions of the estuary. An up-estuary wind of magnitude 0.5 dyne $cm^{-2}$ can turn an originally stratified estuary with an average depth of 5m into a well-mixed estuary. A down-estuary wind produces the opposite effect. Subtidal velocity and salinity fields are found to depend significantly on the wind forcing.

Salinity measurements along the Sandy Hook-Rockaway transect were made during August 20th and 27th, 1980. It is found that the model predicts well the details of the observed salinity distribution. Throughout the tidal cycle, the observations show that unstably stratified water columns are created by advection of waters of different densities which subsequently mix. The observation also shows that the water becomes vertically homogeneous during a spring tidal cycle. These complex three dimensional flow structures and mixing events are predicted remarkably well by the model. There is also good agreement with the observed time-averaged circulation in Raritan Bay.

## 1. Introduction

Mathematical modelling of estuaries and coastal waters is not an easy task. A theoretical approach usually requires simplifying assumptions such as steady state or an ideal estuarine geometry. This results in simpler analyses, some useful solutions and semi-empirical relations can be obtained (see for examples: Hansen and Rattray (1965), Chatwin (1976), Hamrick (1979) and Oey (1984)). Nevertheless, a real estuary is never in a steady state and its coastline geometry and bottom topography are usually very complicated. Estuarine hydrodynamics invlove a wide range of spatial and temporal scales; it is generally not possible to single out one or two preferred scales which can be used to simplify the governing equations.

Some researchers have therefore turned to numerical modellings (see for examples: Hamilton (1975), Festa and Hansen (1976), Johns (1978), Tee (1979), Owen (1980), Oey, Mellor and Hires (1984a, henceforth referred to as OMH) and Sundermann and Lenz (1983)) wherein insufficient computer time and storage generally dictate either a depth-integrated xy-model or a width-averaged xz-model. Again, one can obtain some useful and interesting results from these models but they do not simultaneously cope with significant vertical variations in salinity and velocity and with complex coastline geometry. Tee (1979) used a linear set of equations and separated the vertical deviations of the currents from their vertical averages. The resulting set of equations can be solved efficiently for various vertical algebraic eddy viscosity formlations. He was only interested in the three dimensional tidal current structure, however, and did not consider any vertical and horizontal salinity variations. Owen (1980) used a Galerkin method in the vertical and a finite difference grid in the horizontal to compute three-dimensional tidal current in Bristol Bay, England. Again, no stratification effect was considered. Most of these models use algebraic eddy diffusivity expressions to model the

turbulent mixing and adjust these expressions so that the mean fields fit the observations. These expressions lack some generality and are sometimes measurement-dependent. They probably work well in certain conditions but may fail in slightly altered conditions. Some models are designed for large-scale simulations (the North sea, for example. See Sundermann and Lenz, 1983) and therefore neglect any density gradients caused by fresh water discharges from rivers. Little work has been done, therefore, to simulate a real estuary with three-dimensional velocity and salinity structures. For a more complete review of the present state-of-the-art of numerical modelling in coastal waters, the reader is referred to Blumberg and Oey (1984).

In this paper, we present some results of a real-time, three dimensional numerical simulation of the Hudson-Raritan estuary for the period covering July, August and September, 1980, which happened to cover a period of low river discharges and for which there are velocity and salinity measurements. The Hudson-Raritan estuary is a typical drowned river, partially mixed estuary located in the north-east coast of United States just off New York City (Figure 1). Over the decades commercial needs have prompted buildings of deep channels and narrow straits and have therefore modified the natural bathymetry of the estuary. The major source of fresh water discharge is from the Hudson river and this ranges from about 100 $m^3 s^{-1}$ in dry seasons to about 1800 $m^3 s^{-1}$ in spring. The combined discharge of Raritan and Passaic Rivers ranges from 10 $m^3 s^{-1}$ to 100 $m^3 s^{-1}$. The circulation and salinity distribution in Raritan Bay are particularly influenced by this source of fresh water. The estuary is connected to the Atlantic ocean through the Sandy Hook-Rockaway transect in the southeast and it is connected to Long Island Sound through the East River Strait in the northeast. These are open boundaries where we shall specify sea level elevations and salinity distributions. Another important factor which governs the circulation in certain shallower regions of the estuary is the surface wind stress. Our model also includes this as part of the surface

boundary conditions.

Our primary purpose in undertaking the present research is (i) to study in more detail the mixing, the velocity and salinity structure in the estuary and to understand how these structures might be affected by transient winds and different tidal ranges; (ii) to test the general predictive capability of a fairly sophisticated time-dependent, three dimensional numerical model as it is applied to a real estuary with real tide and wind forcing and river discharge; (iii) to determine the dominant salt dispersion mechanism in the estuary, and to study how the different mechanisms may be related to estuarine geometry, winds, stratification and tides; and (iv) to study the estuarine circulation and salt transport, particularly in their relations to winds and other sub-tidal forcing.

This paper is Part I of a series of three papers and contains some of the results we have obtained under item number (i). Although comparisons of computed and observed salinity distributions along the Sandy Hook-Rockaway Point transect are made in section 4, we shall defer the main bulk of item number (ii), which includes detailed comparisons with observations of time series of velocity and salinity at a number of stations and depths throughout the estuary, to Part II (Oey, Hires and Mellor, 1984, henceforth II) and the results obtained under item number (iii) and portion of (iv) to Part III (Oey, Mellor and Hires, 1984b, henceforth III). The outline of this paper is as follows.

In section 2 we shall describe the numerical model and the associated boundary and initial conditions. We use the finite-difference model originally developed by Blumberg and Mellor (1980, 1983), suitably modified to include rivers and narrow channels as discussed by OMH. The model uses the Mellor and Yamada turbulence model (1982); it responds to tidal forcing, surface winds, and heat flux and evaporation (neglected in the present application) and solves for elevations and for the three dimensional velocity, temperature and

salinity fields. In section 3, we examine the instantaneous fields of velocity and salinity in the estuary and, in particular, their temporal variations and also the variation of eddy diffusivity at two cross sections in the estuary. We shall study the importance of winds in affecting the currents and vertical salinity structure and hence the mixing processes. In section 4, we shall describe a series of salinity measurements obtained by us along the Sandy Hook-Rockaway transect and we shall compare model prediction with these observations. The paper ends with a concluding summary in section 5.

In addition to the present low fresh water discharge simulation, we have also completed a high discharge calculation. We shall publish the results in a separate paper. We note that Oey (1984) has already used some of these numerical results to check the validity of a generalised Hansen-Rattray's theory of salt transport in estuaries.

## 2. The Numerical Method

A detailed description of the numerical algorithm is given in Blumberg and Mellor (1980, 1983). We shall give an outline here. In the present application, it is noteworthy that the model equations do not contain horizontal dispersion terms. The vertical and horizontal resolution are sufficient such that the model explicitly accounts for horizontal dispersion processes due to small scale advection and vertical mixing (Taylor 1954). This will be a subject of Part III.

The model solves the continuity equation

$$U_x + V_y + W_z = 0 \tag{2.1}$$

and Reynolds' momentum equations:

$$U_t + (U^2)_x + (UV)_y + (UW)_z - fV = -P_x/\rho_0 - (\overline{wu})_z \tag{2.2}$$

$$V_t + (UV)_x + (V^2)_y + (VW)_z + fU = -P_y/\rho_0 - (\overline{vw})_z \tag{2.3}$$

$$\rho g = -P_z \tag{2.4}$$

where x is positive eastward, y positive northward and z positive upward; the origin at the mean tidal level; t is time; U+u, V+v and W+w are instantaneous velocities in the x, y and z directions, respectively, where U, V and W denote the ensemble mean velocities and u, v and w the corresponding fluctuating velocities; $\overline{uw}$ and $\overline{vw}$ are turbulent Reynolds stresses defined by

$$(-\overline{uw}, -\overline{vw}) = K_M (U_z, V_z), \tag{2.5}$$

where $K_M$ is the turbulent mixing coefficient for momentum to be defined shortly; f is the Coriolis parameter = $9.57 \times 10^{-5} s^{-1}$; $\rho$ is the mean density and $\rho_0$ is a reference density; g is the acceleration due to gravity and P is the pressure. We have made the hydrostatic assumption in (2.4) and have also neglected any density differences unless these differences are multiplied by gravity.

The equation for the mean salinity S is

$$S_t + (US)_x + (VS)_y + (WS)_z = -(\overline{ws})_z \tag{2.6}$$

where the turbulence salt flux $\overline{ws}$ is defined by

$$-\overline{ws} = K_H S_z \tag{2.7}$$

and $K_H$ is the turbulence mixing coefficient for salt. Equations similar to (2.6) and (2.7) for temperature T may also be solved by the model but have been omitted. The density is related to the salinity and temperature by an equation of state (Fofonoff, 1962):

$$\rho = \rho(T,S) \tag{2.8}$$

where, here, $T=17^0c$.

$K_M$ and $K_H$ are calculated according to the Mellor and Yamada (1982) "level 2.5" turbulence model wherein,

$$K_M = S_M lq, \quad K_H = S_H lq, \tag{2.9}$$

l is the turbulence length scale and $q^2/2$ is the turbulence kinetic energy. They are calculated from turbulence transport equations of the form

$$Df/Dt = (\text{diffusion of f})+(\text{shear and buoyancy productions of f}) +(\text{dissipation of f}) \tag{2.10}$$

where f denotes either $q^2/2$ or $q^2l$. $S_M$ and $S_H$ are stability factors which depend on q, l and the vertical velocity and buoyancy gradients.

Equations (2.1) through (2.10) are cast in finite difference forms and stepped forward in time. The scheme is explicit in the advective transport terms and, because of the generally finer mesh spacing in z, is implicit in the vertical diffusive flux terms. It is formally second order accurate in space and first order accurate in time. The temporal error cannot be large however because of the short time step $\Delta t$ imposed for stability by the Courant condition of the form

$$\Delta t < (1/2)[c^2(1/\Delta x^2 + 1/\Delta y^2)]^{-1/2} \tag{2.11}$$

where $\Delta x$ and $\Delta y$ are the grid sizes in the x and y directions and c is the phase speed of either the free surface gravity wave or the internal gravity wave. A salient feature of the model is the "barotropic-baroclinic" mode splitting technique. Equations (2.1) through (2.4) are vertically integrated

and the barotropic set of equations which result are integrated in time with a short time step determined by $c=(gH_{max})^{1/2}$ in equation (2.11), where $H_{max}$ is the maximum water depth below the mean tidal level. The full three dimensional set of equations are integrated in time with a much longer time step determined by the baroclinic internal wave speed $c_i \approx (gH_{max}\delta\rho/\rho)^{1/2}$; $\delta\rho$ is the top to bottom density difference. In our calculation with $\Delta x=\Delta y=0.53$ km, $\Delta t$ is 15 seconds if c is the surface gravity wave speed and $\Delta t$ is 3 minutes if c is the internal gravity wave speed, both are much smaller than the $M_2$- tidal period of 12.42 hours. The overall numerical scheme is efficient since, for every twelve barotropic calculations, we need only calculate the three dimensional "baroclinic" set of equations once.

The "baroclinic" mode calculation supplies computed bottom friction and vertical integrals of density and vertical variances of horizontal velocity to the barotropic mode calculation. In turn, the barotropic mode calculation supplies surface elevation to the "baroclinic" mode calculation. Details of these implementations are found in Blumberg and Mellor (1980).

Another feature of the model is that the vertical coordinate is a "$\sigma$"-coordinate where

$$\sigma = (z-\zeta)/(H+\zeta)$$

and where $\zeta$ is the surface elevation and H is the depth below the mean tidal level. Thus $\sigma = 0$ at the surface and -1 at the bottom. Irregular bottom topography and a time-dependent surface elevation are accomodated by the model, simply and accurately. For the present application of the model, there are 10 $\sigma$-levels ($\Delta\sigma = 0.1$).

Connections to Jamaica Bay and Small Rivers

For an estuary which consists of broad water regions as well as narrow channels and rivers like the Hudson-Raritan estuary it is impractical to model the narrow waterways three dimensionally and they are therefore modelled by width-averaged equations which are subset of the full three dimensional

equations (2.1) through (2.10). These narrow rivers are stored in computer memory which, otherwise, would correspond to the land areas shown in figure 1 and are therefore included at no additional computer cost. The four rivers and one strait handelled in this way are: the Hudson, Hackensack, Passaic and Raritan Rivers and the East River Strait. Additional matching conditions are imposed at the rivers-bay junctions. Details of these procedures can be found in OMH.

Jamaica Bay has an average depth of about 3m and is further complicated by the presence of small islands and marsh areas. These fine details can barely be resolved by our present model resolution. Since the circulation and salinity distribution inside the bay is not of particular interest to us we decided to model the bay with a constant-depth "bay" of approximately equal volume and store it in computer memory in the land area marked "NEW YORK" in figure 1. Matchings conditions are imposed at the mouth of Jamaica Bay connecting to the main harbour region.

Boundary Conditions

The boundary conditions at the free surface, $z=\zeta(x,y,t)$, are:

$$
\begin{aligned}
K_M(U_z,\ V_z) &= (\tau_{0x},\ \tau_{0y}) \\
K_H(S_z) &= \dot{S} \\
q^2 &= \text{constant}.|\underset{\sim}{\tau}_0| \\
q^2 l &= 0 \\
W &= U\zeta_x + V\zeta_y + \zeta_t
\end{aligned}
$$

where $\underset{\sim}{\tau}_0 = (\tau_{0x}, \tau_{0y})$ is the wind stress vector and $\dot{S} = S(0)(\dot{E}-\dot{P})/\rho_0$ where $(\dot{E}-\dot{P})$ is the net evaporation minus precipitation surface flux rate, which, however, has been set to be zero in the present calculation.

At the bottom the boundary conditions for S, $q^2$ and $q^2 l$ are similar to those at the surface. For W, we have

$$W = -U.H_x - V.H_y, \quad z = -H(x,y)$$

and for U and V we match the computed solutions with the turbulence law of the

wall which extends the computed U and V into the viscous or roughness sublayer where the no slip condition at the ocean floor is satisfied. Thus,

$$(U,V) \sim ((-\overline{wu},-\overline{wv})/ku_*).\ln((H+z)/z_0) \quad \text{as } z \to -H,$$

where $u_*$ is the bottom friction velocity, k=0.40 is von Karman's constant and $z_0$ is the roughness height. For the results in these papers, $z_0$ = 0.2 cm. Sensitivity studies show that an increase of $z_0$ to 1 cm decreases the $M_2$ tidal amplitudes at Sandy Hook and at the Battery by 3% and 7% of the observed amplitudes of 67.9 cm and 68.6 cm, respectively. Thus a precise value of $z_0$ does not appear to have particularly significant influence on the numerical results.

At the open boundaries at the Sandy Hook connection with the Atlantic ocean and at the East River Strait connection with the Long Island Sound, tidal elevations are specified using NOS tidal records at Sandy Hook and at Willets Point. Since the actual open boundary on the eastern region of the model is some 10 km away from Sandy Hook the phase of the tidal record is advanced by about 15 minutes (Swansen, 1976). Figure 2 shows the tidal record used in the model at the Sandy Hook open boundary region. The tide in the estuary is mainly semi-diurnal with the ratio of the amplitudes of the four major constituents $(K_1+O_1)/(M_2+S_2)$ ranges from about 0.12 at Willets Point to about 0.19 at Sandy Hook. During flood, the salinity is linearly interpolated for a duration of one hour from its (computed) value at the end of ebb to a value of 34 ppt along the south eastern open boundary and to a value of 27.3 ppt at the other open boundary at Willets Point. During ebb, the salinity is calculated using an advection equation. The depth-independent salinity value specified during flood is obviously an over simplification of the actual physics. Ideally a salinity boundary condition with vertical structure, obtained from field observation, would have been preferred. Such data is not available, however.

Upstream of rivers, fresh water discharge velocities are specified and

the salinities are set to zero. The fresh water discharges were obtained from U.S. Geological Survey Water - data report. The Hudson River contributes most with a mean discharge of 130 $m^3s^{-1}$ during the simulation period. The Raritan, Passaic and Hackensack Rivers' discharges are much smaller with a total mean of 9 $m^3s^{-1}$. There are four major sewage sources. Two with a combined mean discharge of 11 $m^3s^{-1}$ are near the mouth of Kill van Kull which opens to the upper harbor near the mouth of the Passaic River. A third is in the East River Strait with a mean discharge of 42 $m^3s^{-1}$ and the fourth sewage source is in Jamaica Bay with a mean discharge of 14 $m^3s^{-1}$. All of these are included as "fresh water" model inputs.

The wind record for the simulation period was obtained from John F. Kennedy International (JFK) Airport, New York, and is assumed spacially uniform for the entire estuary. The wind is generally light and southwesterly (wind blowing from the southwest) with speeds rarely exceeding about 10 $ms^{-1}$ (maximum wind stress $\approx$ 1.5 dyne $cm^{-2}$). The wind stress components are shown in figure 3.

Initial Conditions

The calculation was initialized with a zero salinity value in each of the rivers and with a transition layer of length of 5 km near its mouth so that salinity values joined smoothly to ocean values in the main harbor; the latter were specified linear in z with 33 ppt at the surface and 34 ppt at the bottom. The model was spun up from this initial state for 155 days. The fresh water discharge, wind stress and open ocean sea level during this spin-up period were specified cyclicly every 31 days with values corresponding to the July 1980 period. A water parcel would have travelled the entire length of the Hudson river and into the Atlantic Ocean during this spin-up period. Oey (1984) has shown that this spin-up time is sufficient for the salt content in the Hudson River to reach a near equilibrium state independent of the initial salinity distribution. The model was run for another 61 days to cover the

August and September 1980 periods. The entire 216 days' run required about 20 hours on a CDC-Cyber 205 computer, 15% of which was spent on writing computed results on tapes. With more CDC-205 FORTRAN program enhancements it is possible in the future to cut this time to about 10 hours.

## 3. Computed Results

### Tidal Cycle

Figure 4 shows a series of near-surface and near-bottom (the lowest sigma surface, 0.05xdepth from the bottom) velocity vector and salinity contour plots at four instants during an $M_2$ tidal cycle beginning at 05:00, 27 August when the tidal current at the Narrows is at slack, before flood. The phasing of the surface current vector agree well with NOS Tidal Current Chart and also with our simpler two dimensional barotropic calculation (OMH). One notes the markedly different magnitudes between the surface and bottom currents. The vertical velocity shear is significant and therefore is important in affecting the transport of salt, other passive contaminant and sediment. The bottom current can attain a value of about 40 $cms^{-1}$ in the deep channel regions where the depths exceeds 10m but is generally smaller ($\simeq 5$ $cms^{-1}$) in shallower regions.

The salinity contours show two types of distinct features. One type shows relatively smooth salinity distribution and occurs in Raritan Bay where the bottom and coastline bathymetries are slowly varying. Another type shows the formation of patches of waters of different salinities. This occurs across the Sandy Hook-Rockaway transect, through the Narrows and into the upper bay region south of the Battery. The size of a patch is typically of the order of 9 $km^2$ (36 grid points) and is therefore well resolved by the model. The life time of each patch is of the order of a few hours or less (time scale of vertical mixing is $H^2/K_H$, $H \simeq 10m$, $K_H \simeq .01$ $m^2s^{-1}$), suggesting that each patch is formed by horizontal advection and subsequent vertical turbulent mixing, i.e. by shear dispersion processes. This dispersion process is important in determining the circulation and salt distribution in an estuary and cannot be simulated well by numerical models with coarse grid resolution. A particular process of mixing which we shall find to be important is when two fluids of

different salinities converge due to the interaction of the mean velocity fields with irregular bottom and coastline bathymetries. We shall see later from both observation and model results that regions of such intense mixing occur near the tips of Rockaway and Sandy Hook Peninsulas. These are regions where sewage from Jamaica Bay and fresh water from a small stream south of Sandy Hook in the southern boundary of the model domain (Navesink River) are mixed with the ocean water. In the present simulation the Navesink river discharge was not considered to be important since it amounts to only about 1/20th of the discharge from Raritan River. In figure 4 one can only see the sewage plume from Jamaica Bay as it mixes with main harbor's water. As shown in Part III, the interaction of the main harbor's water with the waters from Jamaica Bay and Sandy Hook Bay turns out to be very important in affecting the up-estuary salt transport at the Sandy Hook-Rockaway transect.

In Raritan Bay where the bottom and coastline bathymetries are relatively smooth and where the tidal current is also rather small with maximum magnitude of about 40 $cms^{-1}$, there are not many salinity patches and salinity distribution is smooth. The Coriolis effect is such that the less saline water is on the right hand bank, looking seaward. These salinity contours resemble the surface salinity observations made by Ayers et. al. (1949). Precise comparison is not possible however because (i) the discharge from Raritan River during the period of observation is about 5-10 times larger than the discharge we used for Raritan River during the simulation period and (ii) as we shall see shortly the wind has significant effects on the velocity and salinity distributions in Raritan Bay. The lack of wind information during the observation period make it difficult to interpret the results precisely.

The salinity distribution depends strongly on the three dimensional velocity fields. The most notable example occurs in the Ambrose Channel running through the mid-section of Sandy Hook-Rockaway transect and into the Narrows. In figures 4a,b one sees the 30-31 ppt contours being carried by the

flooding current into the region just south of the Narrows and in figures 4c,d the same contours are carried out into the open ocean by the ebbing tide. Due to density gradients the salinity intrusion during flood is more extensive near the bottom of the channel.

Subtidal Wind Forcing Events

As will be shown in Part III, circulation and sea level in the estuary has significant correlation with the winds at time scales of a few days to weeks. In this subsection, we examine the variations of velocity and salinity in the time scales of a few days. In particular, we single out a period during which there is a significant subtidal variation of wind. One such event occurs from the 15th through the 23rd of August. From the 15-16, the wind is westerly (blowing from the west, see figure 3 and also the two bottom panels in figures 8a,b). The 25-hour averages of velocity and salinity distributions centered around August 15/12:00 are shown in figure 5a. One sees classical two layer estuarine flows occuring throughout the harbor: in the Narrows, near the mouths of Jamaica Bay and all four rivers and in most regions of Raritan Bay. The bottom landward flow is particularly noticable in deep channels. For example, the deep channel running the whole length of Raritan Bay from Sandy Hook to the mouth of Raritan River. The surface to bottom salinity difference is about 1 ppt in most parts of the harbor, but exceeding values of 2 ppt in particular places closed to fresh water sources.

On the 16th of August, the wind starts blowing from the north north-west, reaching a fairly large magnitude of about 1.5 dynes $cm^{-2}$. The 25-h averaged current and salinity centered around August 16/12:00 are shown in figure 5b. The current responds quickly to the wind, as can be seen clearly in Raritan Bay where the surface current turns from an eastward flowing to a southward flowing direction, and there is a corresponding compensating northward flowing bottom current. The salinity is not altered significantly from its previous distribution but there are some changes in Raritan Bay where the contours are

closer together at the southern shore and also along the Ambrose Channel from the mid-section of the Sandy Hook-Rockaway Transect to the Narrows where the bottom salinity is seen to intrude further up north into the estuary, driven by a now stronger two layer gravitational flow in response to the stronger northerly wind.

On August 18 the wind has changed to light south-southwesterly. Figure 5c shows that the current in Raritan Bay again responds rapidly. The salinity in Raritan Bay has also relaxed back to its original distribution shown in figure 5a. The response in deeper regions such as in the Narrows and in Ambrose Channel is slower. For example, note that a short tongue of surface salinity of 29 ppt just south of the Narrows in figure 5a has now elongated further southward, also that the bottom salinity in Ambrose Channel has intruded further north into the estuary, both in response to the strong northerly two days previously.

The wind remains light south-southwesterly until about 6 AM on 20 August when it changes to a fairly strong (0.5 dynes $cm^{-2}$) north-easterly and remains that way until 23 August. Figure 5d shows that the current structure in Raritan Bay has now changed to a "reversed" two layer estuarine circulation, with landward-flowing surface and seaward-flowing bottom currents. Note the change in orientation in the salinity contours in Raritan Bay to a more north-south direction and a more homogeneous vertical and axial (east-west) salinity structure. As we shall see shortly, these homogenieties are brought about by increase in turbulent mixing caused by unstably stratified water columns in the bay. These unstably stratified water columns are induced by the up-estuary (the easterly) wind. Note also the formation of a new tounge of less saline water (the 28.5 ppt salinity contour) just south of the Narrows, and also the more up-estuary intrusion of bottom saline water along the Ambrose Channel, both of which are again in response to the north-easterly wind. From a study of model's subtidal results covering the two months

simulation period, we have found that the intrusion of the tounge of salinity plume from the Narrows to Raritan Bay exists also even in the absence of any significant northerly wind. However, the northerly wind does appear to strengthen further the plume formation and, in many instants, produces deeper intrusion of waters from the Narrows into Raritan Bay. After 23 August, the wind returned to a light south-westerly and the estuary again return to its original state as in figure 5a. The important conclusion is that the subtidal dynamics in the estuary are significant and any attempt to represent the estuary as a steady-state system is bound to be crude and may be erraneous.

Finally, we show in figure 6 a time-depth plot of the low-pass filtered velocity at the mid-station of Sandy Hook-Rockaway transect. Here, the direction of the velocity is defined to be normal to the transect, positive seaward. The filter used has a half-amplitude gain at 34 hours. The $M_2$ tidal amplitude is reduced by $10^{-3}$ after filtering. The original and filtered wind stress in a direction normal to the transect is also shown. We see that the two-layer flow is modified significantly by the wind stress. An up-estuary wind (a southeasterly) around August 14 destroys the two-layer density induced flow on August 15 while a down-estuary wind (a northwesterly) centered around noon, August 16 strengthened the density-induced flow. If the up-estuary wind were stronger (or the local depth more shallow) a reversed two-layer flow similar to that found in Raritan Bay would probably result. One cannot entirely ignore three dimensionality however, since the cross-transect bottom variation is significant in this case.

Temporal Variations of u, S and $K_H$

We next examine a series of instantaneous tangential velocity, normal velocity, salinity and turbulence mixing coefficient contours for one tidal period at the Sandy Hook-Rockaway transect and at a section across Raritan Bay (figure 1). These two sections have very different coastline and bottom bathymetries. A detailed study of velocity and salinity fields at these

sections should therefore provide a better understanding of the differences and similarities of circulation and salt transport caused by variations in channel shape, tidal strength and wind.

Sandy Hook-Rockaway Transect: Cross-section no. 1

As seen in figure 7 this section is about 10 km wide and has an averaged depth of about 8.5 m. It has two deep ship channels: the Ambrose Channel situated at the mid-section with a maximum depth of about 15 m and the Sandy Hook Channel situated near Sandy Hook with a maximum depth of about 12 m.

At 22:00 hours, August 19th, 1980, which corresponds closely to the beginning of flood at this section, the contours of normal velocity, $u_n$, in figure 7a show that flood (negative sign) begins first on the Rockaway side of the section where the maximum velocity is 50 $cms^{-1}$. From earlier plots (not shown) we estimate that the flood on the Rockaway side commences one to one and a half hour earlier than the rest of the section. We note that the near surface velocity above the Ambrose channel is still ebbing (positive sign). The cross-channel velocity $u_T$ (positive to the right) is of the same order as $u_n$, implying significant flow curvature and hence large centrifugal acceleration. The salinity contours show more saline water on the right hand bank (looking landward) and less saline water on the left bank. This is in part caused by the coriolis effect and in part caused by the large cross-channel accelerations. Notice the markedly less saline water near the surface at the right hand bank. This is due to the sewage discharge from Jamaica Bay and the relatively strong stratification that remains from the salinity distribution of the previous ebb. Also notice the large value of $K_H$ in the right hand side of the transect. This large turbulent mixing is not produced by velocity shear which is small at this instant. We have computed the gradient Richardson number

$$Ri = -g\rho_z/\rho_0((U_z)^2 + (V_z)^2)$$

and we find that Ri actually attains a negative (unstable) value at this

instant in this region of the transect. From a detailed study of the instantaneous contours of Ri we find that this unstable stratification repeats itself at the beginning of every flood tide due to a blob of denser water flowing across the transect near the Rockaway point from a shallower region north east of the Rockaway point (see figure 1 for location). When this denser water encounters the less saline near-surface water (see the salinity contours near the right hand side of the section in figure 7a) from the previous ebb, an unstable stratification is created and our turbulence model then calculates large mixing. Whether or not this physical event actually occurs is an interesting question; considering the complex three-dimensionality of the flow it is, however, not unreasonable. For later reference we shall refer to this type of instability as a density-overturning instability.

At 23:00 hours, (figure 7b), the entire cross section is flooding. The largest flood velocity occurs at the Rockaway side while the velocity at the rest of the section is developing into a recognizable boundary layer profile. We note that the flooding velocity near the mid-section is weak and this combines with the strong flooding velocity near the right hand bank to produce the salinity contours which now show large leftward inclination. There are three regions of intense mixing: two near the banks and one in the mid-section above the deep channel. These are produced by the developing flood velocity shears. Ri is less than about 0.05 in these local regions, well below the critical $Ri_c$=0.19 over which the level 2.5-turbulence closure model approximately supresses turbulent mixng. On the two banks, Ri is negative so that the density-overturning instability again plays a role in promoting turbulent mixing.

At 01:00 hour, August 20th (figure 7c), full flooding velocity profiles have developed across the section. The velocity at the Rockaway side has receeded from its maximum flood amplitude. We see the large bottom generated turbulence in the deep channel and across the section. The turbulence is now

mainly due to an almost 3-fold increase in the turbulence kinetic energy (not shown), produced by the large velocity shears. However, density-overturning instability is still evident in the mid-section region, where Ri attains a minimum value of -0.05. The water becomes more vertically homogeneous as shown by the salinity contours.

At 03:00 hours (figure 7d), which is close to the end of flood and the beginning of ebb, the bottom currents are already ebbing at the Rockaway side of the section while the near surface currents are still flooding. In a vertically homogeneous flow the near-bottom boundary layer fluid with less momentum reverses first under an opposing pressure gradient. In the present case of low fresh water discharge and hence weak stratification the horizontal density gradient is not sufficiently strong to sustain a bottom flooding flow during the turn of ebb. The salinity contours show that the "kink" which was previously near the mid-section's surface at 01:00 hour (figure 7c) has been displaced leftward by the (previously) large flood water in the deep channel and in the region to the right of the channel and also by the generally negative cross-channel velocity during the whole flood stage. The cross-sectionally averaged salinity has in fact reached a maximum at this instant.

At 05:00 hours (figure 7e) a full ebb velocity profile has developed. We see the formation of three isohaline "eyes", one above the deep channel in the mid-section and the other two on both sides of the section, at which the salinities are local minimums. These centers of minimum salinity are due to the maximum ebbing velocities at these locations, as shown by the isotach contours. These are also regions where velocity shear is large, but, because of the correspondingly strong stratification ($Ri \approx 0.25$), mixing is small. Relatively large near-surface $K_H$ near the mid-section remains from the intense mixing produced at 04:00 hours (not shown) by the density-overturning instability.

At 07:00 hours (figure 7f) a new salinity minimum is formed on the right

half of the section. Again this is due to the large quantity of less saline sewage water originating in Jamaica bay. This is clearly seen also from the negative cross-channel surface velocity near the right hand bank. The V-shape central channel produces velocity profiles such that there exists a sub-surface jet with velocity magnitude greater than 0.9 $ms^{-1}$ exactly above the deepest portion of the channel. The ebb velocity in the deep channel region is larger than that in the other parts of the cross-section. Despite the large velocity shears, turbulent mixing is inhibited by the strong stratification in most parts of the section, and only become more intense near the left hand bank, where Ri 0.05.

At 09:00 hours (figure 7g) the ebb velocity at the Rockaway side has weakened while that in the part of the cross-section to the left of the deep channel is still quite strong. $K_H$ in the mid-section is very large since Ri is negative and large in magnitude, caused again by the density-overturning instability. As we shall discuss in the next sub-section, there is an easterly, up-estuary wind of magnitude 0.5 dyne $cm^{-2}$ at this instant. As a result the near surface water actually floods before the sub-surface water. This brings in slightly saltier water near the surface and produces an unstable water column.

At 10:00 hours (not shown) flood begins and the subsequent contours are similar to those we have just described (figures 7a through 7g). There is one modification however due to the diurnal inequality of the tide (see for example figure 2b). The tidal cycle which commences at 22:00, August 19th (figure 7a) and ends at 09:00, August 20th (figure 7g) is a low amplitude cycle relatve to the subsequent high amplitude cycle (10:00 through 22:00, August 20th). There is about 35cm difference in tidal range between the two cycles. The larger amplitude, second cycle produces more vigorous mixing and generally less stratification. Figure 7h shows for example the contours at about two hours before the end of flood at 13:00 hours, August 20th. One

should compare this with figure 7c. We see that the "kink" in the salinity contours in figure 7c disappears in figure 7h. The generally larger tidal velocity and intense mixing during this second cycle results in the section becoming vertically homogeneous.

We arrive at the following conclusions:

(i) During times of slack water (end of flood or ebb) water columns often become unstably stratified due to density-overturning caused by advection with subsequent mixing of waters of different densities. Clearly this type of mixing depends in a complicated way on estuarine geometry and bottom topography. The instability, though infrequent and less intense, also occurs during the entire flood stage. Thus, in addition to the bottom generated turbulence by the shearing velocity, this type of instability can contribute significantly to the mixing process in an estuary. Moreover, up-estuary wind can also produce density-overturning instability and hence large mixing. This phenomenon is more clearly seen in the Raritan bay, which we shall discuss in the next sub-section.

(ii) The diurnal inequality produces varying amplitudes during subsequent tidal periods. We estimate that the differences in range and the r.m.s. tidal velocity $v_T$ are about 35 cm and 10 $cms^{-1}$, respectively. During the large amplitude period the mixing is intense and the section is less stratified at maximum flood and ebb. As shown in figures 7c and 7h the large amplitude flood can destroy any vertical salinity structure. It may seem surprising that a difference in tidal speed of only 10 $cms^{-1}$ can bring about such large changes in the vertical salinity structure. Fischer (1976) noted that $Ri_E = g(\Delta\rho/\rho)Q_f/(v_T^3.B)$ is a measure of stratification in estuaries, where $\Delta\rho$ is the density of the ocean water, $Q_f$ is the rate of fresh water discharge and B is the width of the section. Because of the cubic power in $v_T$, $Ri_E$ is sensitive to small variations in $v_T$.

(iii) There are large cross-channel flows with significant vertical shears. $u_T$

is largest near the side of the section and this is due to the strong eddies shed from the Rockaway and the Sandy Hook peninsulas (see tidal current figures in OMH). The sides of the section are also sites of intense turbulent mixings.

(iv) There is a strong interaction between the main bay and Jamaica Bay. The less saline sewage water from Jamaica Bay is "flushed" into the main bay and into the Atlantic ocean by way of the intense eddies which are shed from Rockaway Peninsula. As we shall see in Part III, this mechanism is important to the upstream salt transport across the section.

Raritan Bay: Cross-section no. 2

This cross-section is about 10 km wide and has an averaged depth of about 5 m. The velocity , salinity and turbulence mixing coefficient contours are shown in figures 8a through 8h. Some features of the velocity and salinity fields are similar to those shown in figure 7. There are important differences, however.

Since the tide in Raritan Bay is approximately a standing-wave type and since the bay is generally shallow, the tidal current amplitude decreases to a value of about 30 $cms^{-1}$ from its value of about 70 $cms^{-1}$ near the Sandy Hook-Rockaway transect. Therefore, turbulence production by the shearing tidal current is small. Moreover, the generally gentler varying bottom topography and smoother coastlines in Raritan Bay, together with small fresh water discharge from Raritan river result in less mixing of waters of different densities (density-overturning instability can still be induced by winds, however, as we shall see shortly). Overall $K_H$ is about an order of magnitude smaller in Raritan Bay than in the Sandy Hook-Rockaway transect.

The absence of any significant coastline land protrusions means that large eddies are not generated near the sides of the section. Consequently the "trapping" mechanism which allows exchange of waters between the main cross-section and the coastline irregularities is not effective. On the other

hand, vertical deviations in both the velocity and salinity extend nearly the full breadth of the section and we expect significant contributions to the salt balance from their correlation.

Since Raritan Bay is shallow and since the tidal currents are weak the effects of wind are important. In figure 3, we see that the east-west component of the wind changed from positive, down-estuary values to negative values at about 05:00 hours, August 20th. The up-estuary wind was relatively strong and persisted until the 22nd of August. This wind event produced a "non-classical" two layer, non-tidal flow in which the surface layer of water flowed up-estuary while the bottom layer of water flowed down-estuary. We shall study non-tidal circulations in more detail in Part II. Here we show how wind can change the instantaneous tidal currents. Figures 8a (August 19, 22:00 hours, before the up-estuary wind event) and 8g (August 20, 09:00 hours, the beginning of up-estuary wind event) correspond closely to the time of the beginning of flood. We see from figure 8a that the bottom water in the deep channel floods before the surface water. This is a commonly known situation and is due to either the bottom friction or horizontal density gradient or both. In figure 8g, there are three layers above the deep channel, the flooding surface and bottom layers and the ebbing middle layer. The flooding surface layer is due to the up-estuary wind. We can also see this effect from the plots of the $K_H$ contours, which in figure 8g show a surface layer with large mixing. Figure 8h shows the fields at about three hours after the flood and, when compared with figure 8c, shows clearly the effect of up-estuary wind in producing large mixing and vertically homogeneous water columns.

To see more clearly how the up-estuary wind destroys vertical density stratification and hence produces more vigorous vertical mixing we show in figure 9a time-depth plots of deviations of velocity and salinity from their vertical averages ($=f_{sv}+f_{pv}$ defined in Part III, where f denotes either u or S) in the mid-position of the cross-section for the period August 19th 12:00

hours to August 24th 12:00 hours. The x and y-component wind stresses covering the same period are also shown. From 8/19/12:00 through about 8/20/06:00 the wind was relatively calm and to the north ($\tau_{0x} \approx 0$ and $\tau_{0y} > 0$). In this period the zero salinity deviation contour lowered to about the mid-depth of the water column during the ebb and rose closer to the water surface during flood. A stable density stratification persisted throughout this period. The velocity deviation contour showed positive values near the surface and negative values near the bottom during the ebb and just the opposite during the flood. From 8/20/06:00 through about 8/23/12:00 the wind changed direction and blew to the southwest. The average wind stress was about 0.5 dyne $cm^{-2}$. There appears to be some adjustment period near the beginning and the end of the up-estuary wind event during which there were short periods of stable stratification. In the main period of the up-estuary wind event the stratification was unstable and large turbulent mixing was produced (see for example figure 8h, which is for August 20th, 13:00 hours). Thus, even a light wind in a shallow estuary like Raritan Bay with small tidal r.m.s velocity can have large effects on the stratification and the mixing processes.

For a section in the Narrows (section no. 3 in figure 1) where $V_T \approx 1$ $ms^{-1}$ and $H \approx 15$ m we expect that the wind has less influence on the vertical salinity structure. We illustrate this in figure 8b where we see that stable stratification persisted throughout periods of up-estuary wind event (wind blowing to the north for 8/14/12:00 < time <8/15/08:00 and for 8/17/15:00 < time < 8/20/05:00). We see also that the effect of wind on the velocity shear is small in comparison with the shear produced by the tidal currents. Wind-induced turbulence is produced more by advective destabalization and not because it produces them by vertical velocity shear. Indeed, a down-estuary wind can reduce mixing by generating more stable stratification.

Clearly, one cannot neglect wind effects are important to assess the circulation and mixing in a shallow estuary.

## 4. PRELIMINARY COMPARISON WITH OBSERVATIONS

As stated in the Introduction, we shall defer to Part II the main bulk of comparison of the numerical results with observations. In this section it is, however, appropriate to discuss some observational evidence which were obtained by us and which can be compared with the numerical results presented in section 3.

### 4.1 Observational Procedure

Temperature and conductivity measurements were taken on a boat using Beckman RS-5 salinometer and Martek Mark V water quality analyser at seven, more or less evenly spaced stations along the Sandy Hook-Rockaway transect (figure 1). The vertical (z-direction) spacing at each station was approximately 1.6m with the first meter reading taken at 1.6m below the water surface. Measurements were repeated at about 1.5 hour intervals at each station over a tidal cycle on the 6th, 20th and 27th of August 1980.

### 4.2 Comparison of Salinity Contours at the Transect

In order to compare the observed and the computed salinity distributions at a particular instant of time, a linear, time interpolation of observed values at each observation point was used. This and the fact that the locations of measurement stations are not aligned exactly along a straight line at the Sandy Hook-Rockaway transect introduce possible sources of discrepancy in the comparison. We shall present the comparison results for the 20th and the 27th August periods which represent respectively a neap and a spring tide sample. Thus the effect of different tidal amplitudes on stratification can also be seen.

Figures 10a,b show comparisons of computed and observed salinity contours at approximately slack before flood (August 20, 10:00 and August 27, 16:00). The values of the observed salinity are also given on the observed contour plots. Figure 10a shows that the model predicts well the "U"-shape salinity

contour in the mid-section. More significantly are the occurences of several unstable stratifications in the observed salinity contours. For example, at about 5m below the surface near the Sandy Hook side of the cross-section the vertical difference in salinity (upper salinity - lower salinity) is +0.14 ppt. Also, near the Rockaway Point side of the cross-section the near-surface, vertical salinity difference is +0.11 ppt and the near-bottom, vertical salinity difference is +0.18 ppt. Our salinity measurements are accurate to within 0.01 ppt and so differences greater than $\pm$0.01 ppt in the observed salinity are significant. The model predicts the instabilities near the Rockaway side but misses the instability near the Sandy Hook side, although here the model's salinity is homogeneous vertically (the corresponding gradient Richardson numders Ri are given on the computed plots). We must note that the fact the model does not compute the temperature does introduce a small error in calculated density gradients. However, we have examined the observed density fields which also show the occurence of these instabilities. The model predicts quite well also the vertical and transverse salinity differences except that it misses the observed pool of near-surface, rather fresh water ($\approx$28-28.5 ppt) close to Sandy Hook. We suspect that this is due to the neglect in the model calculation of the Navesink River discharge just south of Sandy Hook on the southern portion of the model boundary. Its total discharge amounts to only 1/20th of the discharge from Raritan River but its close proximity may exert a local influence. Near the Rockaway side, the model predicts a near-surface, rather fresh pool of water ($S \approx 29.5$ ppt) which as discussed before in section 3 is due to the sewage discharge from Jamaica Bay. The observed salinity does not show this feature. One should note however that this fresh pool of surface water was predicted to occur at a depth of less than 2 meters or so below the mean tide level and could therefore be easily missed by the rather coarse vertical resolution used in the observation. We note also that the near-surface (< 2m) observed salinity at observation

station 7 is less than the salinity at station 6, suggesting that there is lesssaline water close to the Rockaway Peninsula shore line flowing out from Jamaica Bay during the previous ebb cycle. It appears that the model over-predicts the amount of sewage water from Jamaica Bay. Our estimate of 14 $m^3s^{-1}$ of sewage from Jamaica Bay is based on the 1980 Report of the Interstate Sanitation Commission. The discrepancy may be due to evaporation from the large marsh areas in Jamaica Bay.

The observed slack-before-flood, spring tide data in figure 10b shows that the water becomes approximately vertically homogeneous. The model predicts this feature rather well, including the slight "kink" in the near-surface salinity contour at the mid-section. The model again predicts well the occurence of unstable stratification in the near surface water close to Rockaway Point but misses the one at about 7m below the surface near Sandy Hook. The model predicts a thin vertical column of rather fresh water ($S \approx 29.0$ ppt) close to Rockaway Point, which is also observed; although the observation does not show such low salinity. There is also evidence of less saline water close to Sandy Hook which is again missed by the model. Excluding these thin columns of less saline water, the transverse salinity difference is predicted well by the model.

Figures 10c,d show the comparisons of computed and observed salinity contours at approximately slack before ebb (August 20, 15:00 and August 27, 10:00). The model predicts well the formation of near-surface isohaline "eye" at the mid-section. Locations where the water column become unstably stratified are predicted well by the model (figure 10c), so are the transverse and vertical differences of salinity. The observation does not show the rather fresh, near-surface water at the Rockaway side however.

Finally, in figure 10d, the model again predicts well the near-surface "eye" of isohalines at the mid-section and the locations of unstably stratified water columns near Rockaway side and also at the mid-section but

misses the one near Sandy Hook side. Again, note that the observed salinity at station 7 is less than that at station 6. This feature is also predicted by the model, although the model salinity is lower than that observed (model salinity = 30.5 ppt; observed salinity = 31.39 ppt). The transverse and vertical salinity differences are predicted well by the model also.

4.3 Discussion

The model predicts remarkably well the spatial and temporal occurences of unstably stratified water columns. Since these instabilities are caused by large scale convergence of waters of different densities, they depend therefore on the detailed three dimensional coastline and bottom bathymetries and also on the surface wind. These important features appear to have been depicted rather well by the model. Note that these good predictions depend not only on a good simulation of the large scale mean velocity and salinity fields, but also on a good parameterization of the turbulence field. We are pleasantly surprised that our simulation can indeed reproduce such detailed physical features of the flow field.

Detailed overall shapes of the salinity contours are also predicted well by the model. These shapes depend largely on the velocity fields and on the vertical turbulent diffusion of salt, which we believe are also simulated well by the model.

Discrepancies between model and observed salinities do exist. These can largely be explained by the errors we made in specifying the "correct" amount of fresh water discharges from small streams and sewage sources. We do not consider these small sources of fresh water to be important in governing the overall dynamics and salt fluxes at the transect. They are apparently significant in local regions however.

4.4 Time-averaged Circulation in Raritan Bay

Figures 11a,b show two pictures of near-surface circulations in Raritan Bay from Jefferies (1962) and Abood (1972) inferred from accumulated salinity

and velocity observations. Although the two pictures are different in many fine details, they do share some common global features. Both pictures show a general seaward flow near the southern shore of the bay. Both show a seaward flow from the Narrows through the Sandy Hook-Rockaway transect and intrusion of water from the Narrows into the mouth of Raritan Bay, although the intrusion in Abood's picture is more clearly indicated.

As we discussed previously in section 3 the circulation in Raritan Bay varies considerably over subtidal time scales of a few days primarily in response to wind forcing. Comparison of model results with Jefferies and Aboods's data is crude since both observations and model results correspond to different wind conditions; however, their observations were mainly taken during the Summer months. Thus they should share some similarities with our simulated results, provided that the simulated results are averaged over long enough time interval. Figure 12 shows a six days averaged circulation obtained from the model and centered around August 12. The wind during this period is light and southwesterly, typical of the wind condition in the bay during Summer. The simulated circulation is seen to share most of the global features inferred from the observations. It appears that the model result more closely resembles Abood's picture of the circulation, especially with regard to the intrusion of water from the Narrows into the mouth of Raritan Bay. The model also predicts the observed north-westerly flow near the northern shore of the bay, apparently induced by the predominat south-westerly wind. The model fails to predict the clockwise gyre south of Sandy Hook, as implied by Abood's picture. But here the model result agrees with Jefferies' picture that there should be a northward flow along the western shore of Sandy Hook Peninsula. This northward flow can be the result of the fresh water discharge from Navisink River south of Sandy Hook on the New Jersey side of the model domain. The model result suggests, however, even in the absence of this discharge, the boundary constraint of Sandy Hook Peninsula should also produce the observed

northward flow.

## 5. Conclusions

Using real sea level and wind forcing and real river discharges we have numerically simulated the time dependent, three dimensional velocity and salinity structures in the Hudson-Raritan estuary, covering the July through September period of 1980. We also compared the computed synoptic salinity fields with observations along the Sandy Hook-Rockaway Point transect and the time-averaged circulation in Raritan Bay. The principal results of this paper are:

1. Computed surface (bottom) salinity contours show that patches of water of constant salinity are produced in regions of estuary where there are complex coastline and bottom bathymetries. These eddies are apparently induced by the interaction of the time-dependent three dimensional velocity fields with bathymetry. The eddies are advected and subsequently mixed throughout the vertical water columns. These are important physical processes which contribute to shear dispersion in an estuary.

2. The model predicts that convergences of water masses of different densities by the three-dimensional velocity field can produce unstably stratified water columns and lead to intense mixing which supplement the turbulent mixing produced by the velocity shears. This physical process is supported by observed salinity distributions along the Sandy Hook-Rockaway transect. The model predicts well the spacial and temporal locations of these unstably stratified water columns and intense mixing. Model results also indicate that the instability occurs more often during flood than during ebb stage, presumably because of the large amount of denser water entering the estuary during flood. Thus for the low discharge period which we have simulated the mixing is generally more intense during the flood than it is during the ebb.

3. Unsteady winds are important in changing the vertical velocity and

salinity structures, which in turn change the turbulent mixing in the estuary and would therefore affect the up-estuary salt transport. Both the two-dimensional, horizontal "barotropic" circulation and the vertical, gravitationally induced circulation vary considerably with wind forcing at subtidal time scales. For the rather light wind stress ($\approx$0.5 dyne $cm^{-2}$) during the simulation period, the subtidal variations in the velocity and salinity fields are most significant in Raritan Bay where the local average depth is less than 5m.

4. Both observed and computed salinity distributions show that the water changes from a vertically stratified state to a vertically homogeneous state when the tide changes from a neap cycle to a spring cycle.

The significant subtidal signal we have found in our results make it difficult to properly define a statistically equilibrium estuary with short observational record. Results and conclusions obtained from short-record data for defining an "average" condition in an estuary are therefore suspect. We shall elaborate on this point in Part III.

The good agreement of the model results with observations is encouraging, although the model does contain some simplifying assumptions. For example, at observation station 4 at the Sandy Hook-Rockaway transect (figure 1), the observed temperature taken during August 20 and 27 show that the maximum top to bottom difference can be as much as 6 $^{o}C$. This produces a density difference which would be effectively caused by a salinity difference of about 1.5 ppt. The observed salinity difference at the transect can be as much as 3 ppt, whereas the model's salinity difference at the same location across the transect has values of at most 2.8 ppt. Thus the local error in density difference can be as much as 30-40% and would certainly affect the local subtidal, density-induced circulation.

Other possible errors exist due to uncertainties in the open boundary specifications and the value of the bottom roughness parameter $z_o$. Our

sensitivity studies indicate that the latter error is not serious. A good estimate of $z_o$ is still desirable but can be quite complicated since $z_o$ depends not only on the bottom topographic fine structure, but also on short-period surface waves (Grant and Madsen, 1979). Other physical mechanisms like surface heat flux and evaporation/percipitation, which are neglected in the model, may also be important.

Acknowledgements

We wish to thank Drs. A. Blumberg and K. Bryan for reading the first draft of the manuscript and for giving many valuable comments. The figures were drafted by P. Tunison and processed by J. Conner. This research was sponsored by the New Jersey Sea Grant program under a grant from the Office of Sea Grant of NOAA, Grant no. 81 AA-D-0065, Project no. R/E-3. Additional funding was provided under Grant no. NA 80 RAD 00033 from the Northeast Office of the Office of Marine Pollution Assessment of NOAA. LYO was supported in part by the Visiting Scientist Program of Princeton University/NOAA, Grant 04-7-022-44017.

References

Abood, K.A. (1972). Circulation in the Hudson Estuary. Paper presented at Hudson Estuary Colloquium, 23 February, City College CUNY, N.Y.

Ayers, J.C., Ketchum, B.H. and Redfield, A.C. (1949). Report to Middlesex County Planning Board on hydrographical considerations relative to the location of sewer outfalls in Raritan Bay. Tech. Rep. Ref. No. 49-13, WHOI.

Bloomfield, P. (1976). Fourier Analysis of Time Series: An Introduction. John Wiley & Sons, Inc. New York.

Blumberg, A.F., and Mellor, G.L. (1980). A coastal ocean numerical model. In "Lecture Notes on Coastal and Estuarine Studies, 1" (J. Sundermann and K.P. Holz eds.). Springer-Verlag, New York.

Blumberg, A.F., and Mellor, G.L. (1983). Diagnostic and prognostic numerical circulation studies of the South Atlantic Bight. J. Geophys. Res. 88, 4579-4592.

Blumberg, A.F., and Oey, L-Y. (1984). Modelling circulation and mixing in estuaries and coastal oceans. Submitted to Adv. in Geophys.

Bowman, M.J., and Wunderlich, L.D. (1977). Hydrographic Properties. MESA New York Atlas Monograph 1, New York Sea Grant Institute, Albany, New York.

Chatwin, P.C. (1976). Some remarks on the maintenance of the salinity distribution in estuaries. Estuarine & Coastal Mar. Sci. 4, 555-566.

Doyle, B.E., and Wilson, R.E. (1978). Lateral dynamic balance in the Sandy Hook to Rockaway Point transect. Estuarine & Coastal Mar. Sci. 6, 165-174.

Elliott, A.J. (1978). Observations of meteorologically induced circulation in the Potomac estuary. Estuarine & Coastal Mar. Sci. 6, 285-299.

Festa, J.F. and Hansen, V.H. (1976). A two-dimensional model of estuarine circulation: the effects of altering depth and river discharge. Estuarine

& Coastal Mar. Sci. 4, 309-323.

Fischer, H.B. (1972). Mass transport mechanisms in partially stratified estuaries. J. Fluid Mech. 53, 671-687.

Fischer, H.B. (1976). Mixing and dispersion in estuaries. Ann. Rev. Fluid Mech. 8, 107-133.

Fischer, H.B., List, E.J., Koh, R.C.Y., Imberger, J. and Brooks, N.H. (1979). Mixing in inland and coastal waters. Academic Press, New York.

Fofonoff, N.P. (1962). Physical properties of sea-water, in The Sea, vol. 1, 3-30, Interscience, New York.

Grant, W.D. and Madsen, O.S. (1979). Combined wave and current interaction with a rough bottom. J. Geophys. Res. 84, 1797-1808.

Hamilton, P. (1975). A numerical model of the vertical circulation of tidal estuaries and its application to the Rotterdam waterway. Geophys. J. R. astr. Soc. 40, 1-21.

Hamrick, J.M. (1979). Salinity intrusion and gravitational circulation in partially stratified estuaries. PhD thesis. University of California, Berkeley, California.

Hansen, D.V. and Rattray, M. (1965). Gravitational circulation in straits and estuaries. J. Mar. Res., 23, 104-122.

Hires, R.I., Oey, L-Y and Mellor, G.L. (1984). Numerical model study of the tidal hydraulics of Raritan Bay. In press, Bulletian of the New Jersey Academy of Science.

Holley, E.R., Harleman, D.R.F., and Fischer, H.B. (1970). Dispersion in homogeneous estuary flow. J. Hydraul. Div. Proc. ASCE, 96, 1691-1709.

Hunkins, K. (1981). Salt dispersion in the Hudson estuary. J. Phys. Oceanog. 11, 729-738.

Jefferies, H.P. (1962). Environmental characteristics of Raritan Bay, a polluted estuary. Limnol. Oceanogr. 7, 21-31.

Johns, B. (1978). The modeling of tidal flow in a channel using a turbulence

energy closure scheme. J. Phys. Ocenogr. 8, 1042-1049.

Longuet-Higgins, M.S. (1969). On the transport of mass by time-varying ocean currents. Deep-Sea Res., 16, 431-447.

Mellor, G.L., and Yamada, T. (1982). Development of a turbulence closure model for geophysical fluid problems. Rev. Geophy. Space Phy., 20, 851-875.

Oey, L-Y. (1984). On steady salinity distribution and circulation in partially mixed and well mixed estuaries. In press, J. Phys. Oceanogr.

Oey, L-Y, Hires, R.I. and Mellor, G.L. (1984). A three-dimensional simulation of the Hudson-Raritan estuary II: comparison with observation.

Oey, L-Y., Mellor, G.L. and Hires, R.I. (1984a). Tidal modelling of the Hudson-Raritan estuary. In press, Estuarine, Coastal & shelf Science.

Oey, L-Y., Mellor, G.L. and Hires, R.I. (1984b). A three-dimensional simulation of the Hudson-Raritan estuary III: salt flux analyses.

Owen, A. (1980). A three-dimensional model of the Bristol channel. J. Phys. Oceanogr. 10, 1290-1302.

Pritchard, D.W. (1978). What have recent observations obtained for adjustment and verification of numerical models revealed about the dynamics and kinematics of estuaries? In "Estuarine Transport Processes" (B. Kjerfve, ed.), pp.1-10. University of South Carolina Press, Columbia, South Carolina.

Sundermann, J. and Lenz, W. (1983). North sea dynamics. Springer-Verlag, New York.

Swansen, R.L. (1976). Tides. Mesa New York Bight Atlas Monograph 4, New York Sea Grant Institute, Albany, New York.

Taylor, G.I. (1954). The dispersion of matter in turbulent flow through a pipe. Proc. R. Soc. London Ser. A223, 446-468.

Tee, K-T. (1979). The structure of three-dimensional currents. Part I:

Oscillating currents. J.Phys. Oceanogr. 9, 930-944.

List of Figures

1. The location map and the computational model region of the Hudson-Raritan estuary. Depth contours are in meters below the mean tide level. Rivers are also included in the calculation but they are not shown here in the figure in order that we may show greater details of the main estuary. The calculation in the East River strait (shown near the north eastern boundary) ends at the Willets Point, some 18 km beyond the northern model boundary of the strait shown here. Jamaica Bay is also included in the model, using the land storage region marked NEW YORK in the figure. Details of these implementations can be found in Oey, Mellor and Hires, 1984a. The triangular symbols across the Sandy Hook-Rockaway transect denote stations where salinity measurements were taken on 20 and 27 August.
2. Tidal elevation record (in meters above mean tide level) at Sandy Hook tide station for July through September, 1980. This record and another one at the Willets Point, East River strait, are used as open ocean boundary conditions in the model.
3. Wind stresses (dynes.cm$^{-2}$, positive eastward and northward) at JFK airport for July through September, 1980; (a) east-west component; (b) north-south component. In the calculation these wind stresses are assumed uniform spatially for the entire modelled region.
4. Computed surface and bottom (sigma = -0.95 surface, 0.05xdepth from the bottom) velocity vector and salinity contour plots when the vertically integrated current at the Narrows is approximately at (a) slack before flood; (b) 3 hours later; (c) slack before ebb and (d) 3 hours later. The arrows are plotted at every other grid points.
5. Computed 25H-LP surface and bottom velocity vector and salinity contour plots centered at 12:00 noon on August (a) 15th; (b) 16th; (c) 18th and

(d) 22nd. Average wind direction for each period is also shown.

6. Time-depth contour plot of low-pass filtered velocity at a mid-station at the Sandy Hook-Rockaway transect. The velocity is normal to the transect, positive seaward. Both the original and low-passed wind stress components normal to the transect are also shown in the top panel.

7a. Computed Contours at 22:00 hours near the beginning of flood, August 19th, 1980, of the velocity $u_T$ (positive to the right) the normal velocity $u_n$ (positive ebbing), both in $cms^{-1}$, the salinity S in ppt and the turbulence mixing coefficient $K_H$ for salt in $cm^2s^{-1}$ at the Sandy Hook-Rockaway Point transect. The heavy dotted line denotes values of 30 $cms^{-1}$ for $u_T$, 50 $cms^{-1}$ for $u_n$, 30 ppt for S and 400 $cm^2s^{-1}$ for $K_H$. The heavy solid line denotes values of 0 $cms^{-1}$ for $u_T$ and $u_n$, 29 ppt for S and 200 $cm^2s^{-1}$ for $K_H$. The light dotted line denotes values of -30 $cms^{-1}$ for $u_T$, -50 $cms^{-1}$ for $u_n$, 28 ppt for S and 100 $cm^2s^{-1}$ for $K_H$. The contour intervals are: 10 $cms^{-1}$ for $u_T$ and $u_n$, 0.25 ppt for S and 50 $cm^2s^{-1}$ for $K_H$.

7b. Contours at 23:00 hours, August 19th.

7c. Contours at 01:00 hour, August 20th.

7d. Contours at 03:00 hours near the beginning of ebb.

7e. Contours at 05:00 hours.

7f. Contours at 07:00 hours.

7g. Contours at 09:00 hours.

7h. Contours at 13:00 hours.

8. Caption same as figure 7 but for a section in Raritan Bay. The heavy dotted line denotes values of 10 $cms^{-1}$ for $u_T$ and for $u_n$, 28.5 ppt for S and 25 $cm^2s^{-1}$ for $K_H$. The heavy solid line denotes values of 0 $cms^{-1}$ for $u_T$ and $u_n$, 28 ppt for S and 15 $cm^2s^{-1}$ for $K_H$. The light dotted line denotes values of -10 $cms^{-1}$ for $u_T$ and for $u_n$, 27.5 ppt for S and 5 $cm^2s^{-1}$ for $K_H$. The contour intervals are: 2.5 $cms^{-1}$ for $u_T$ and $u_n$, 0.1

ppt for S and 2.5 $cm^2 s^{-1}$ for $K_H$.

9a. Time-depth plots of deviations of velocity ($cms^{-1}$, top pannel) and salinity (ppt, second pannel from the top) from their vertical averages in the mid-position of the cross-section in the Raritan bay. The heavy solid contour lines denote zero values of either the velocity or the salinity deviations. Ebbing periods are marked by the letter "E" on the top of the figure. The axial wind stress (third pannel from the top) and the cross-channel wind stress (bottom pannel) in $dynes.cm^{-2}$ are also shown.

9b. Same as figure 9a but now at a mid-position of the cross-section in the Narrows covering a different period of up-estuary wind event.

10. Comparison of computed (left panel) and observed salinity distributions across the Sandy Hook-Rockaway transect. The hatched areas are where the water columns are unstably stratified. The computed gradient Richardson numbers Ri are also shown. (a) August 20, 10:00; (b) August 27, 16:00; (c) August 20, 15:00; (d) August 27, 10:00. (a) and (b) correspond approximately to slack before flood and (c) and (d) to slack before ebb.

11. Near-surface residual circulation in Raritan Bay inferred by (a) Jefferies (1962) and (b) Abood (1972), from accumulated observations made mostly during the Summer season when the wind is predominantly light south-westerly.

12. Six days time-averaged computed surface circulation in the estuary. The time average is centered at 00:00 on August 12. The wind during this period is light south-westerly, typical of the Summer wind condition in the estuary.

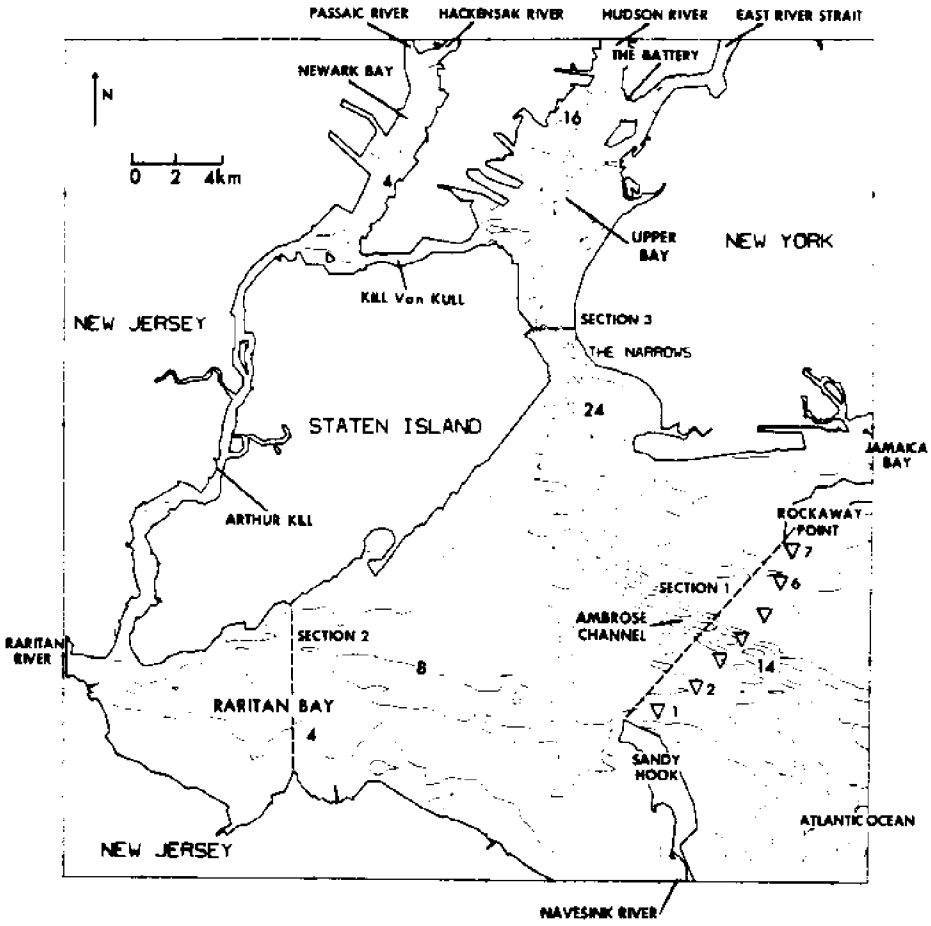


Figure 1. The location map and the computational model region of the Hudson-Raritan estuary. Depth contours are in meters below the mean tide level. Rivers are also included in the calculation but they are not shown here in the figure in order that we may show greater details of the main estuary. The calculation in the East River strait (shown near the north eastern boundary) ends at the Willets Point, some 18 km beyond the northern model boundary of the strait shown here. Jamaica Bay is also included in the model, using the land storage region marked NEW YORK in the figure. Details of these implementations can be found in Oey, Mellor and Hires, 1984a. The triangular symbols across the Sandy Hook-Rockaway transect denote stations where salinity measurements were taken on 20 and 27 August.

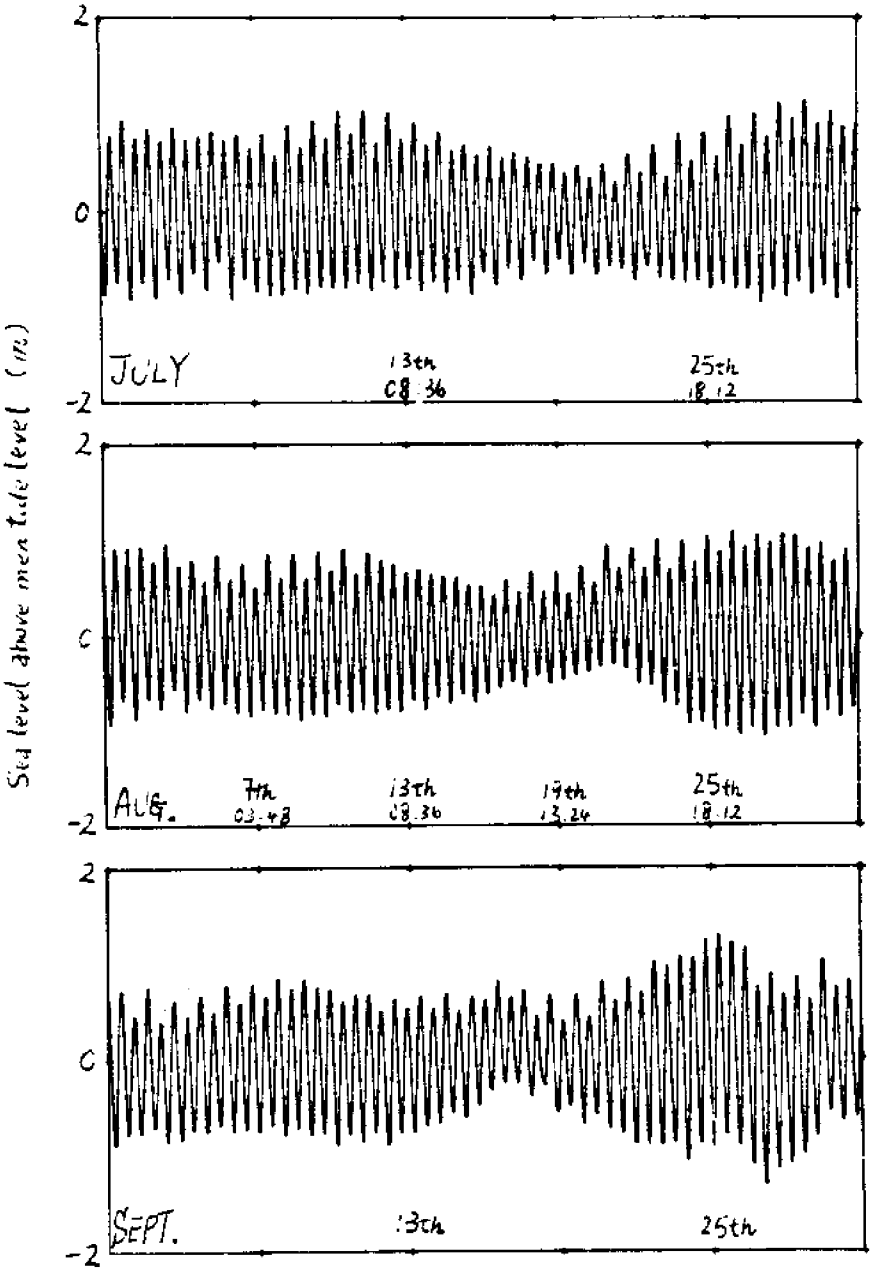


Figure 2. Tidal elevation record (in meters above mean tide level) at Sandy Hook tide station for July through September, 1980. This record and another one at the Willets Point, East River strait, are used as open ocean boundary conditions in the model.

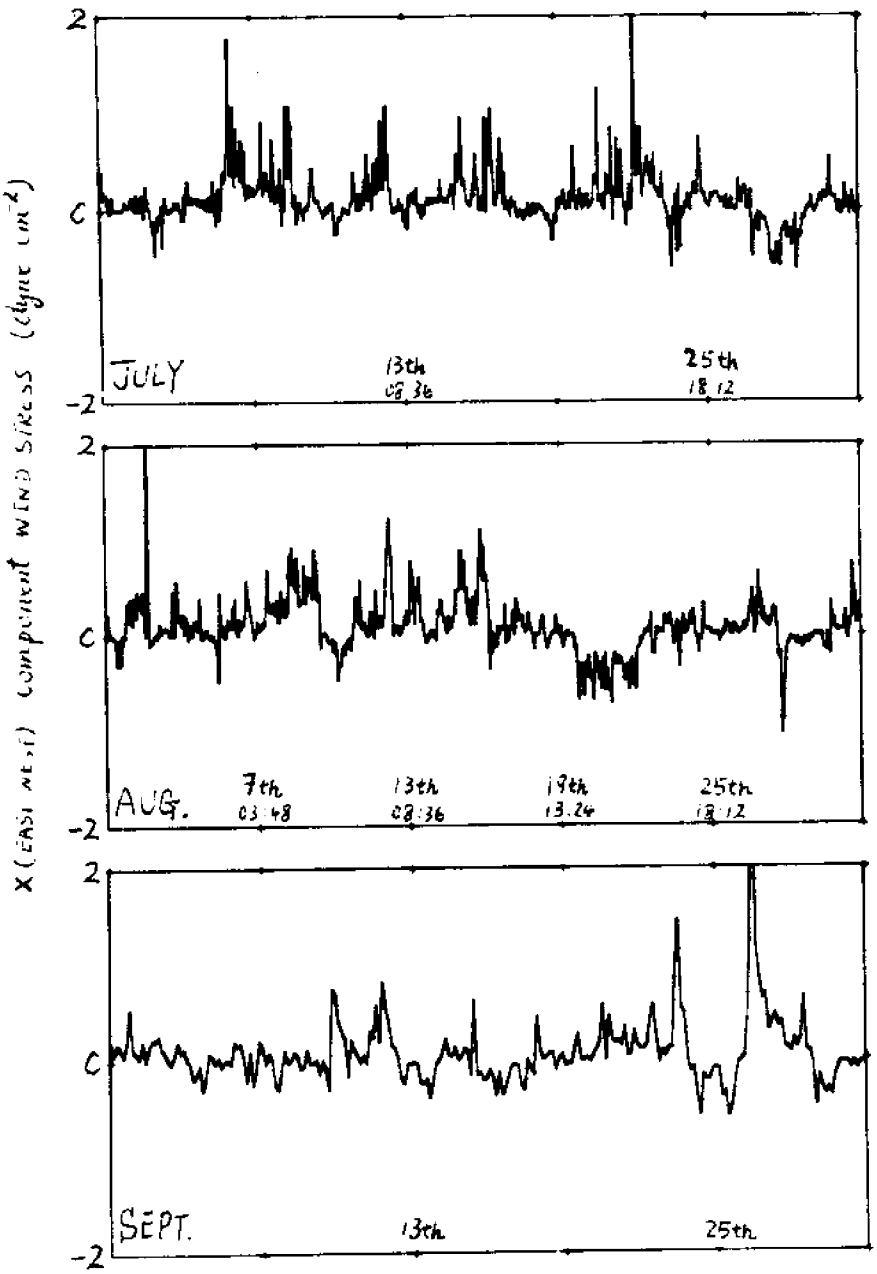


Figure 3 . Wind stresses (dynes.cm$^{-2}$, positive eastward and northward) at JFK airport for July through September, 1980; (a) east-west component; (b) north-south component. In the calculation these wind stresses are assumed uniform spatially for the entire modelled region.

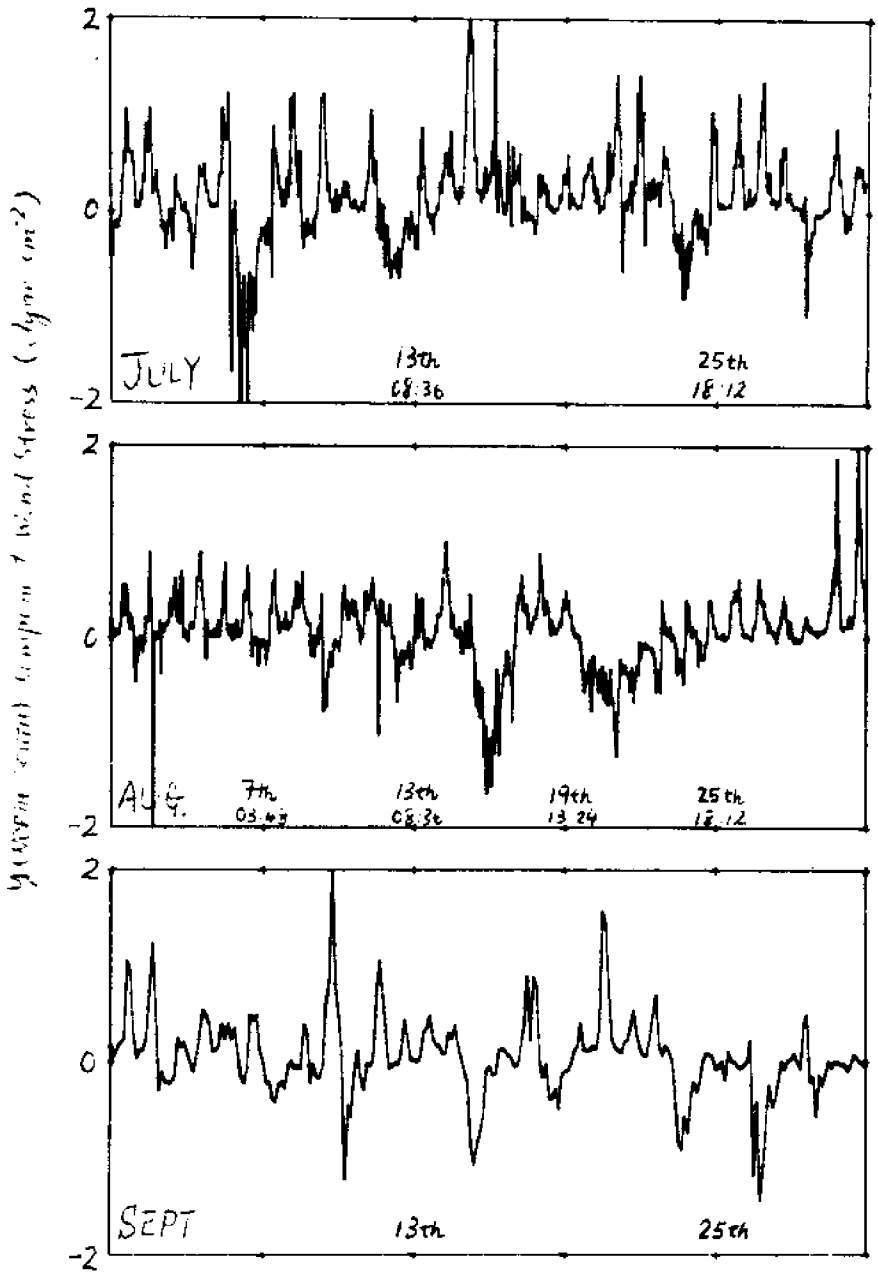
2
0
-2
JULY
13th
08:36
25th
18:12
AUG
7th
03:49
13th
08:36
19th
13:24
25th
18:12
SEPT
13th
25th

Figure 3b.

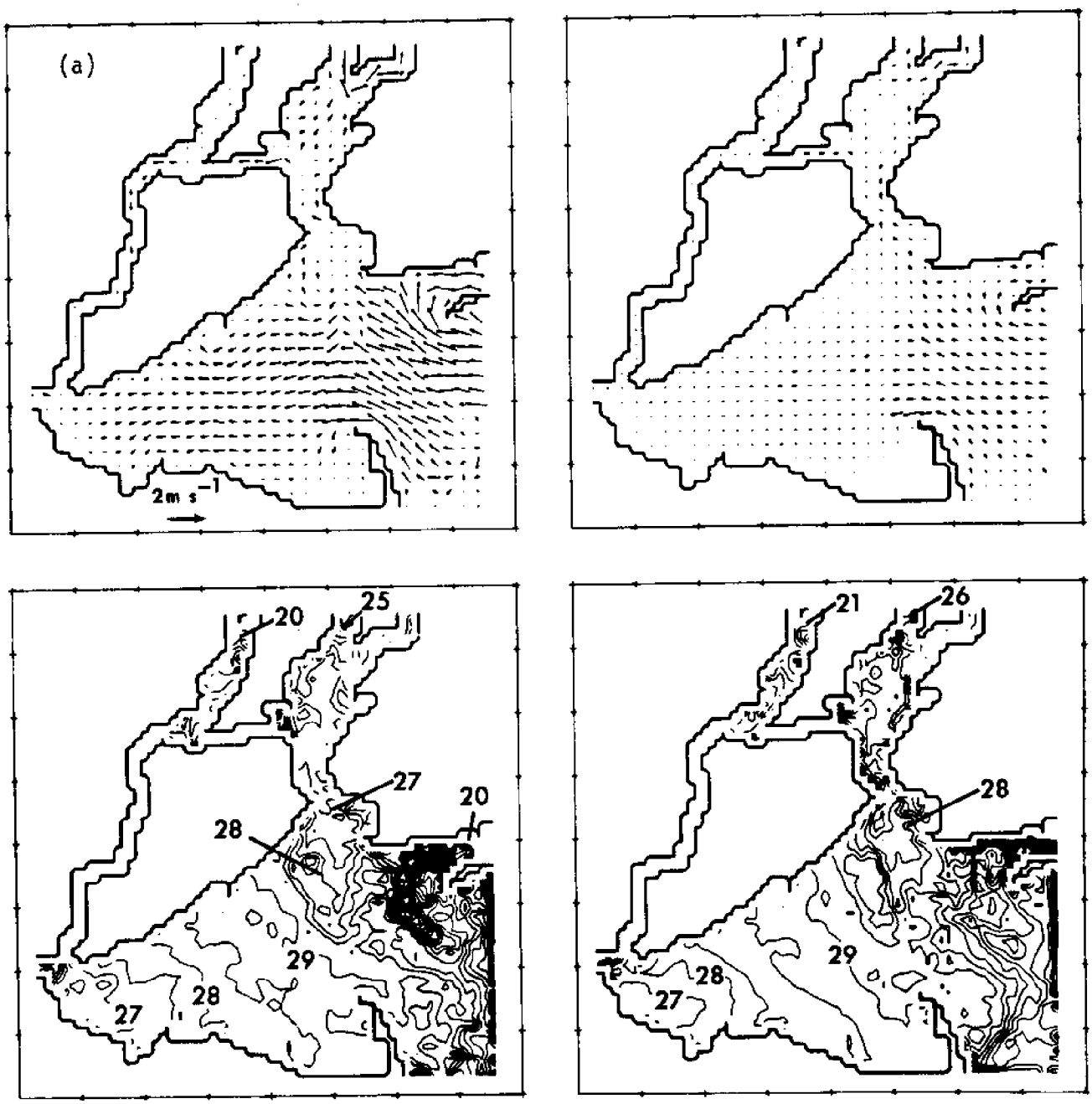


Figure 4 . Computed surface and bottom (sigma = -0.95 surface, 0.05xdepth from the bottom) velocity vector and salinity contour plots when the vertically integrated current at the Narrows is approximately at (a) slack before flood; (b) 3 hours later; (c) slack before ebb and (d) 3 hours later. The arrows are plotted at every other grid points.

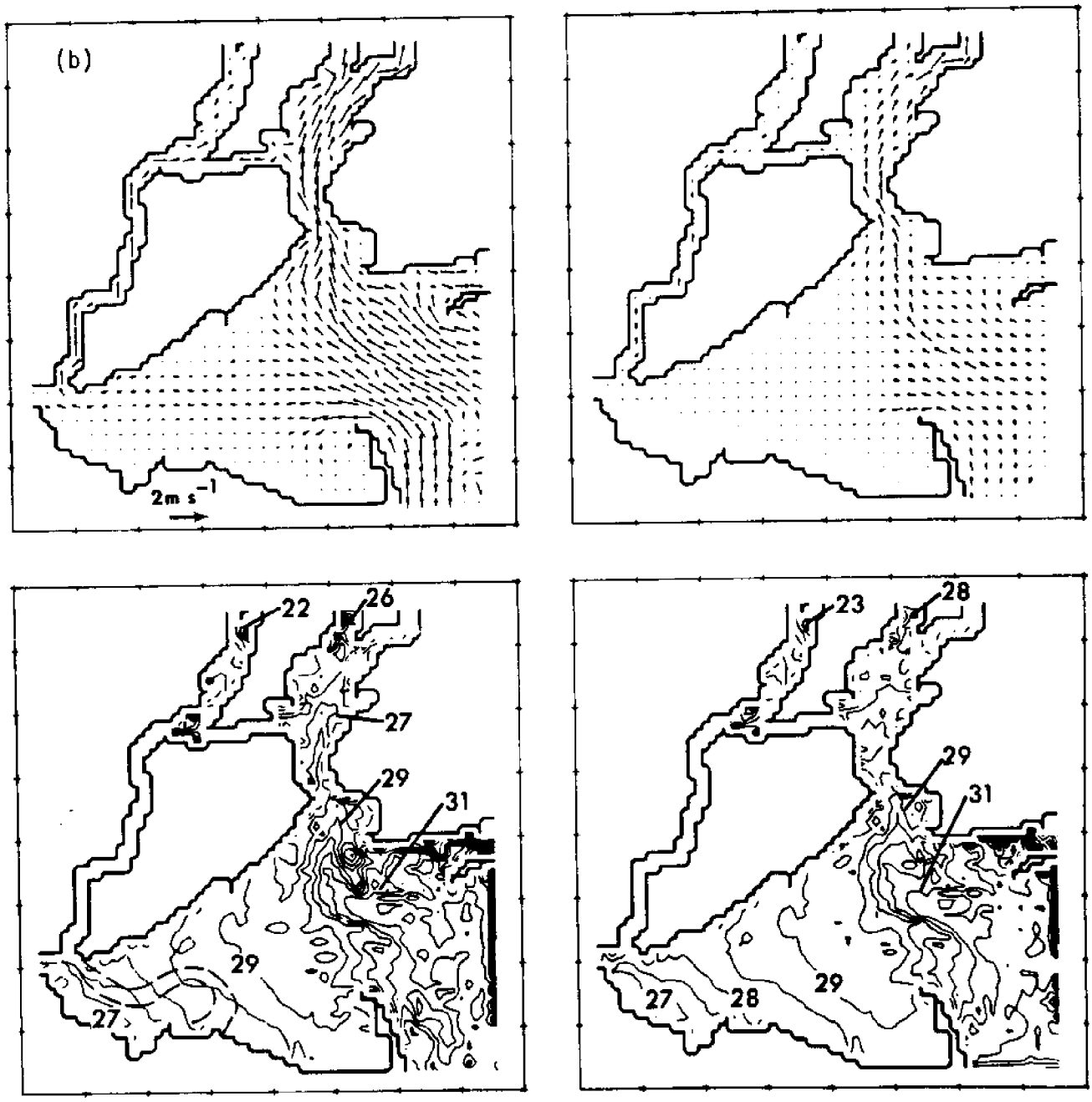


Figure 4b.

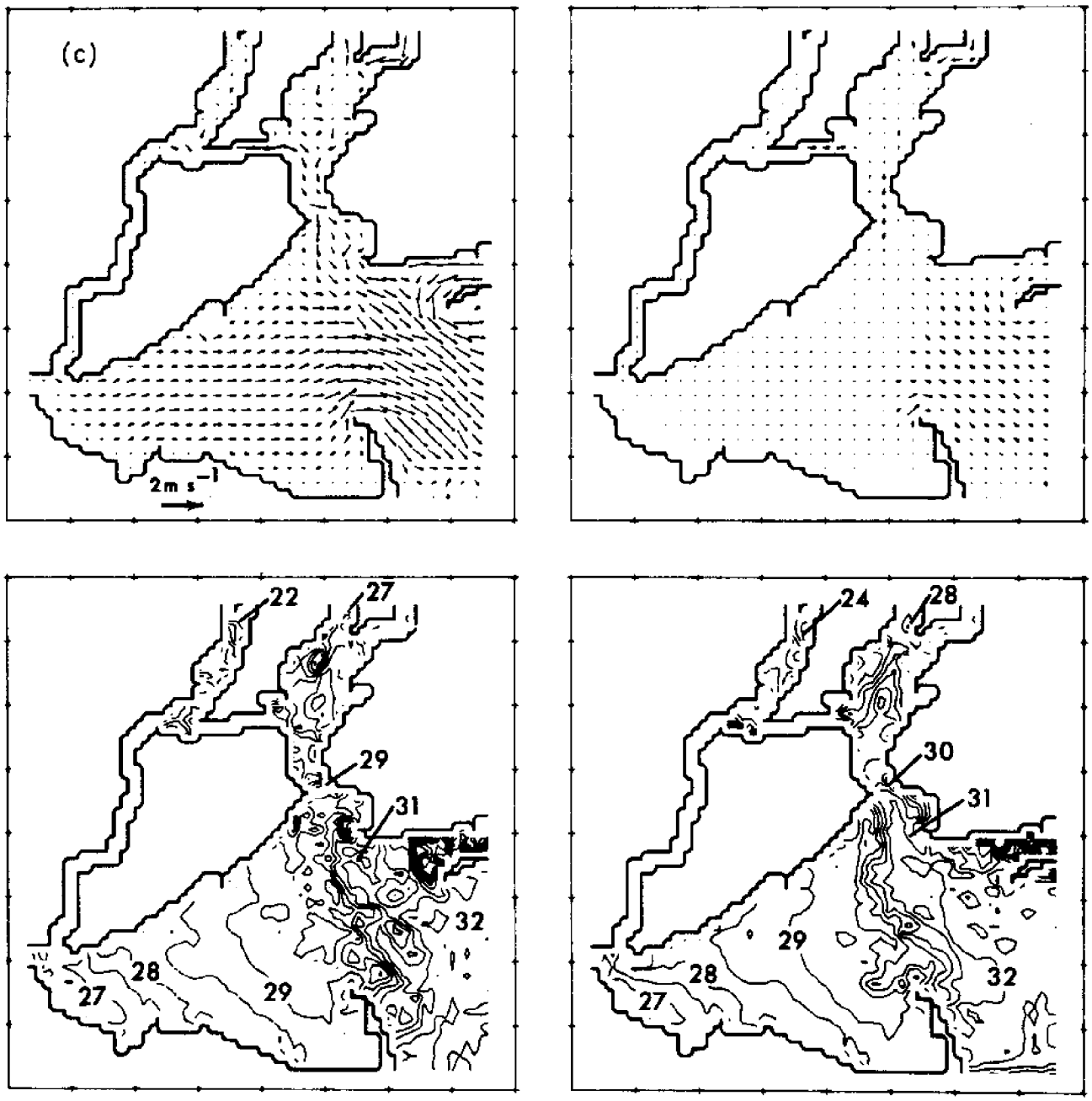


Figure 4c.

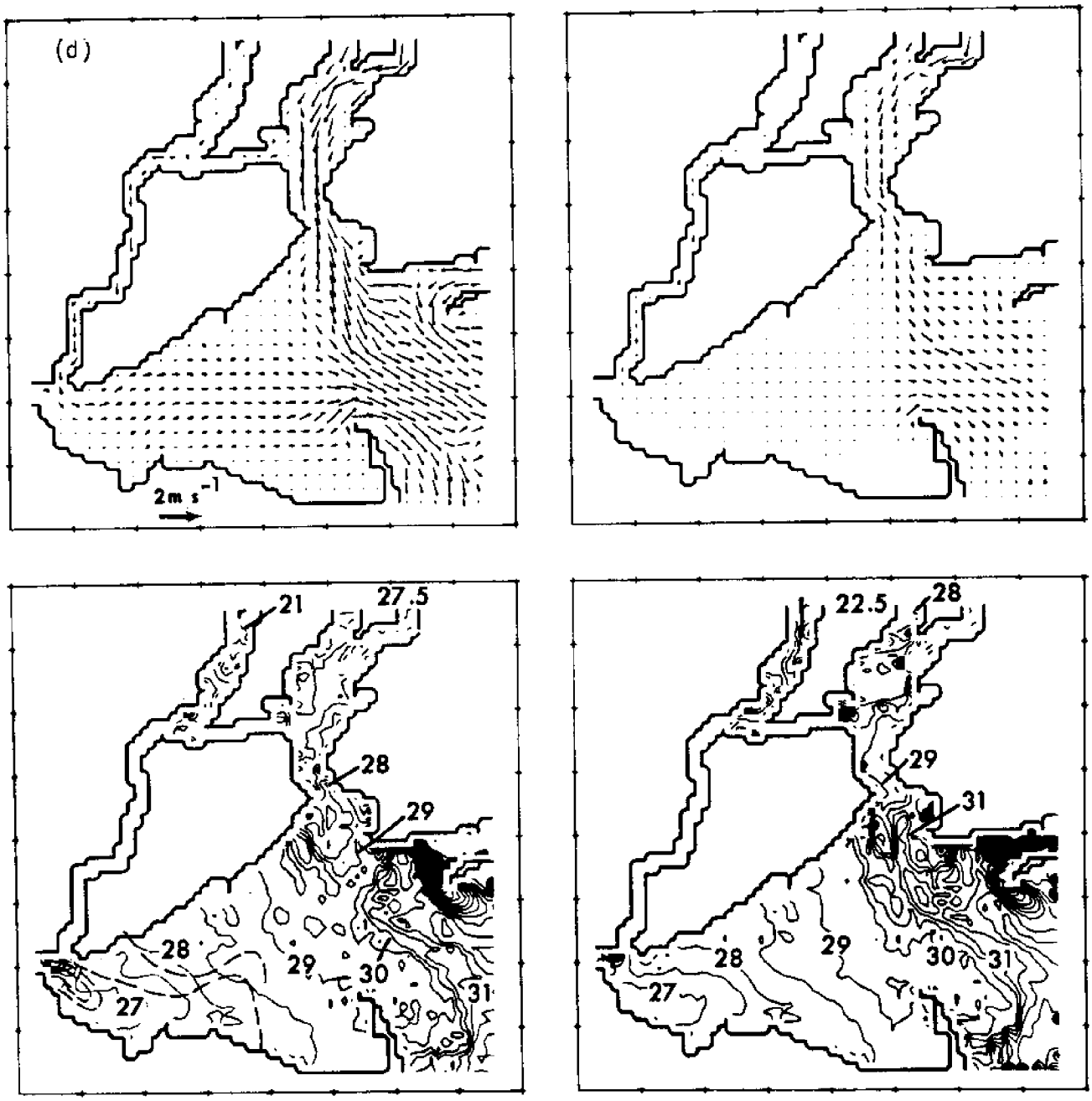


Figure 4d.

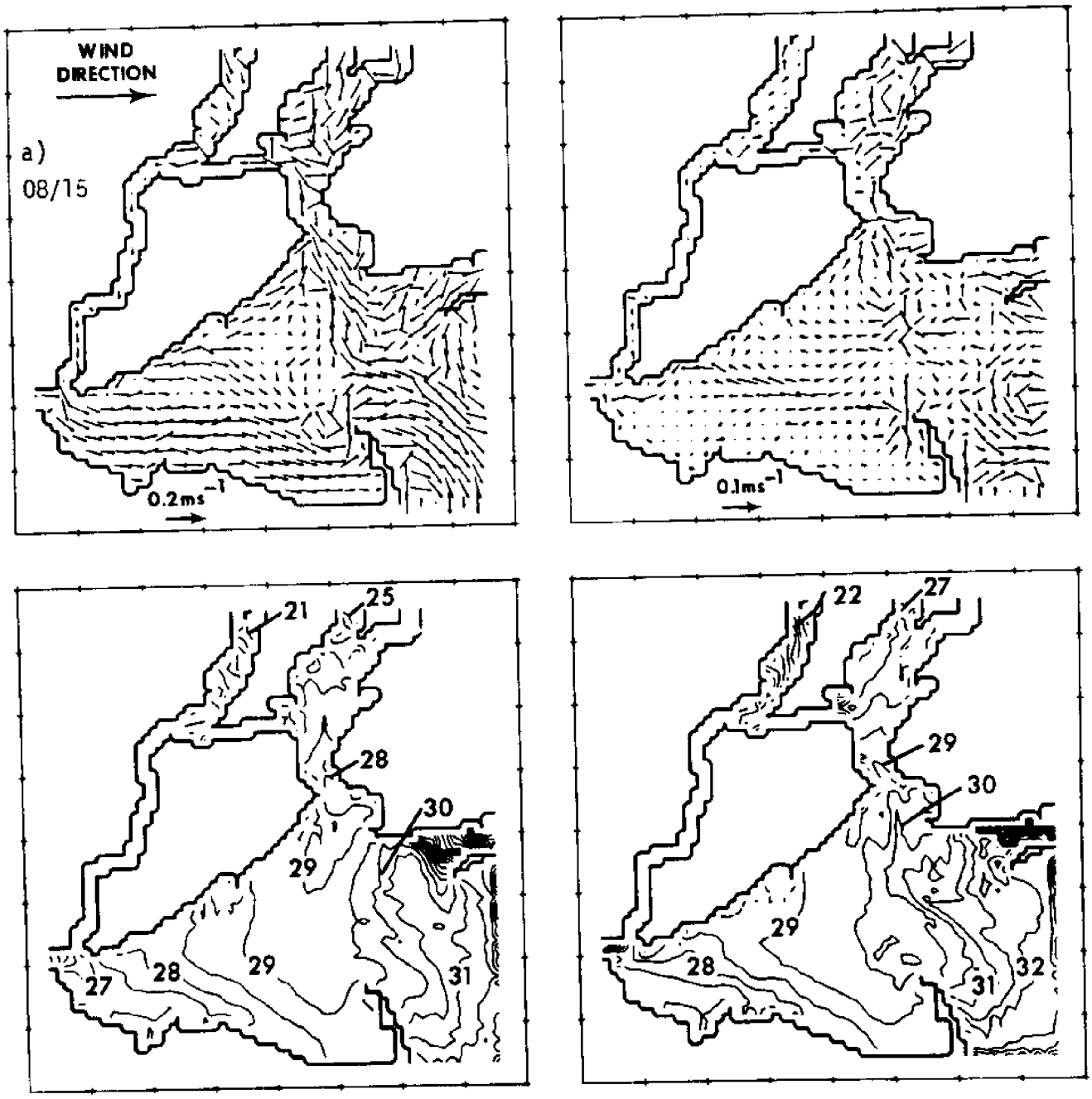


Figure 5 . Computed 25H-LP surface and bottom velocity vector and salinity contour plots centered at 12:00 noon on August (a) 15th; (b) 16th; (c) 18th and (d) 22nd. Average wind direction for each period is also shown.

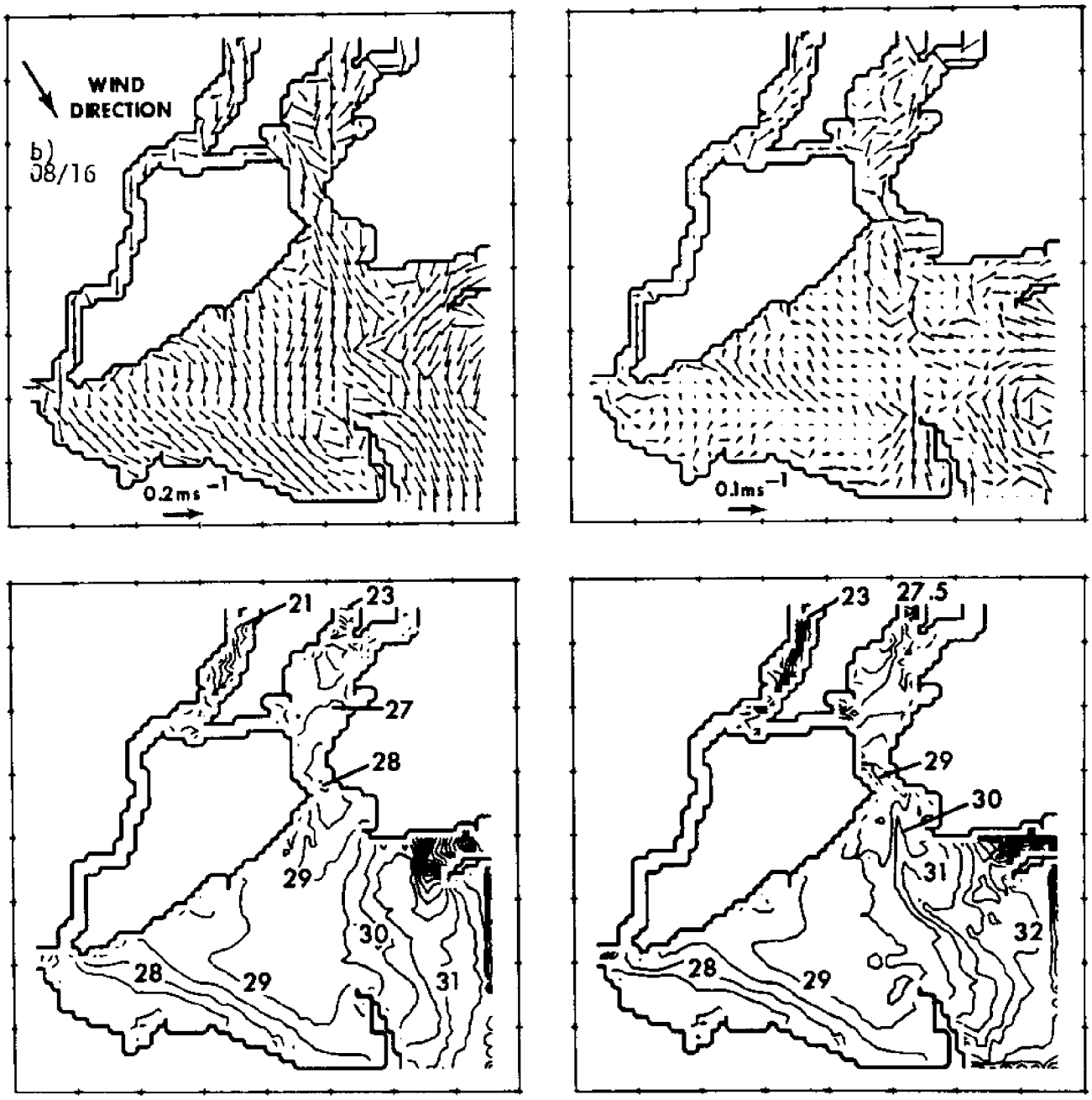
WIND DIRECTION
b)
08/16
0.2ms⁻¹
0.1ms⁻¹
21
23
27
28
29
30
31
28
29
23
27.5
29
30
31
32
28
29

Figure 5b.

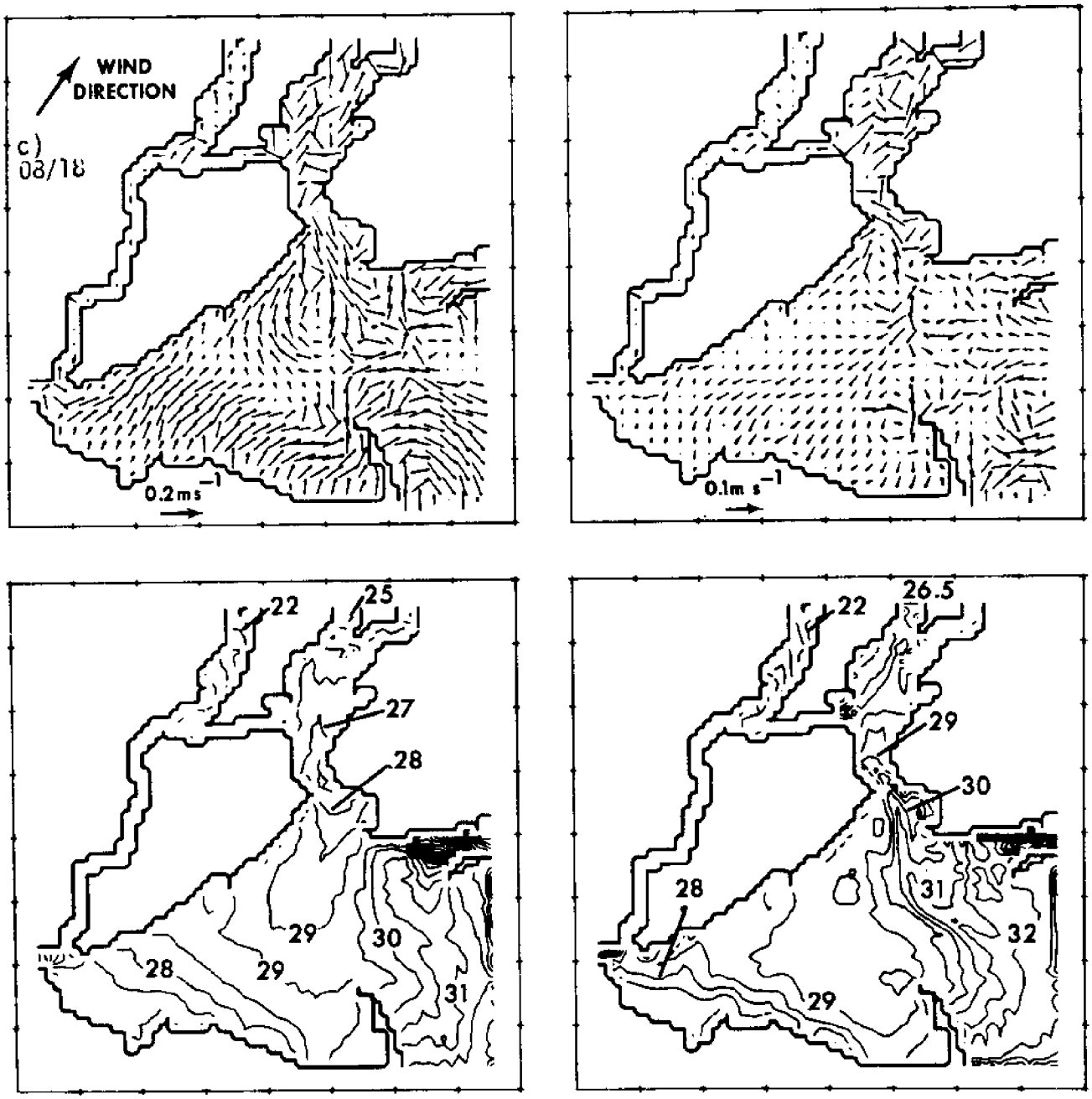
WIND DIRECTION
c)
08/18
0.2ms⁻¹
0.1m s⁻¹
22
25
27
28
29
30
31
28
29
22
26.5
29
30
28
31
32
29

Figure 5c.

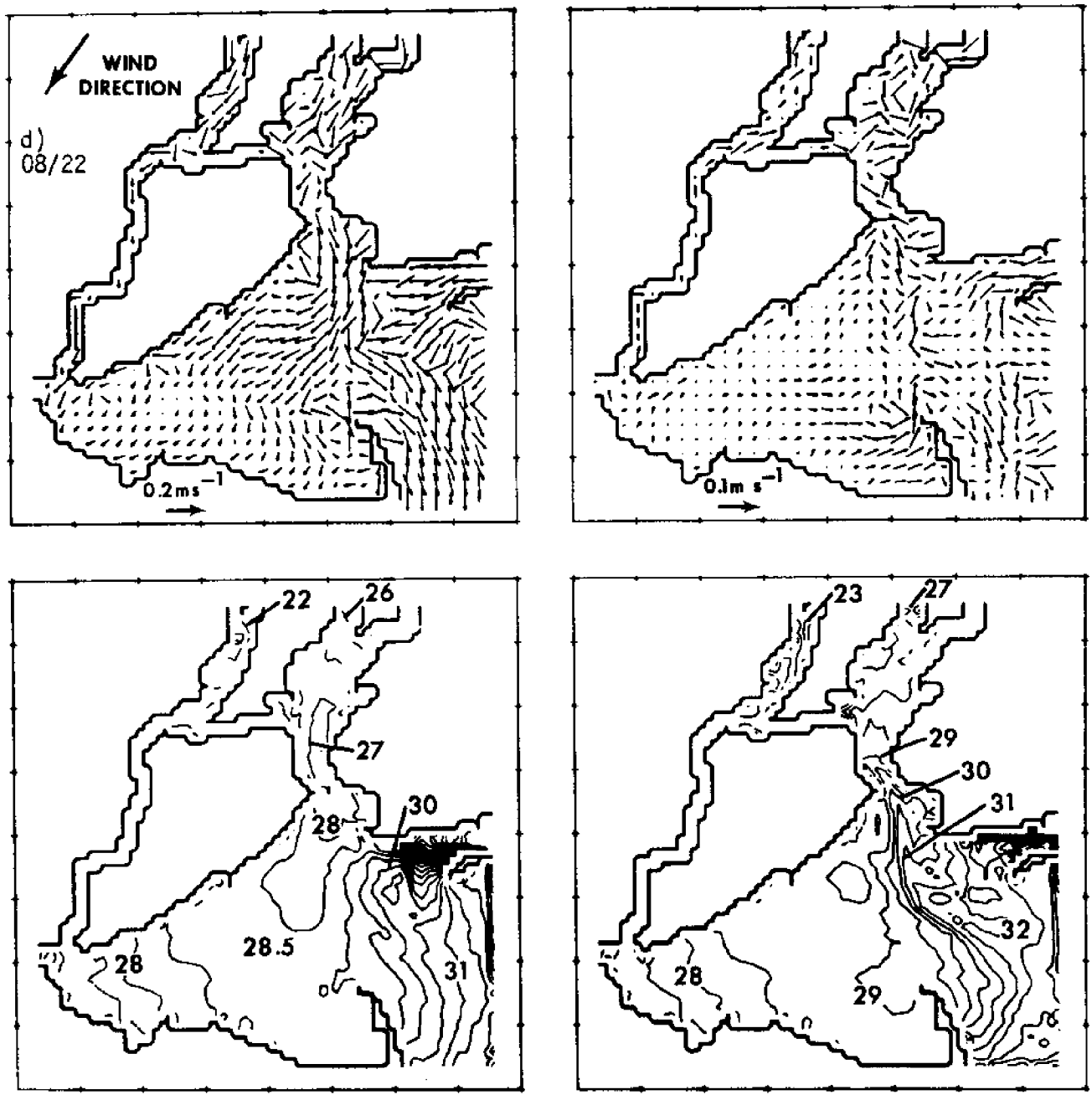
WIND
DIRECTION
d)
08/22
0.2ms⁻¹
0.1m s⁻¹
22
26
27
28
30
28
28.5
31
23
27
29
30
31
32
28
29

Figure 5d.

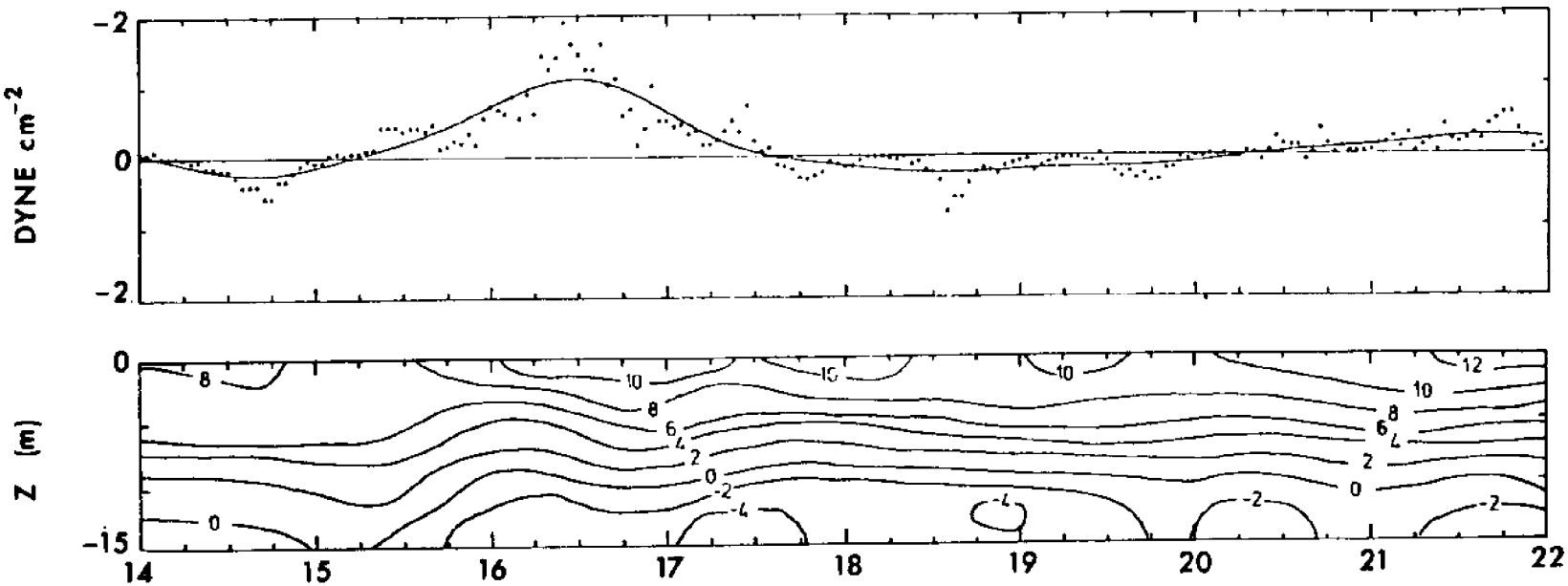


Figure 6. Time-depth contour plot of low-pass filtered velocity at a mid-station at the Sandy Hook-Rockaway transect. The velocity is normal to the transect, positive seaward. Both the original and low-passed wind stress components normal to the transect are also shown in the top panel.

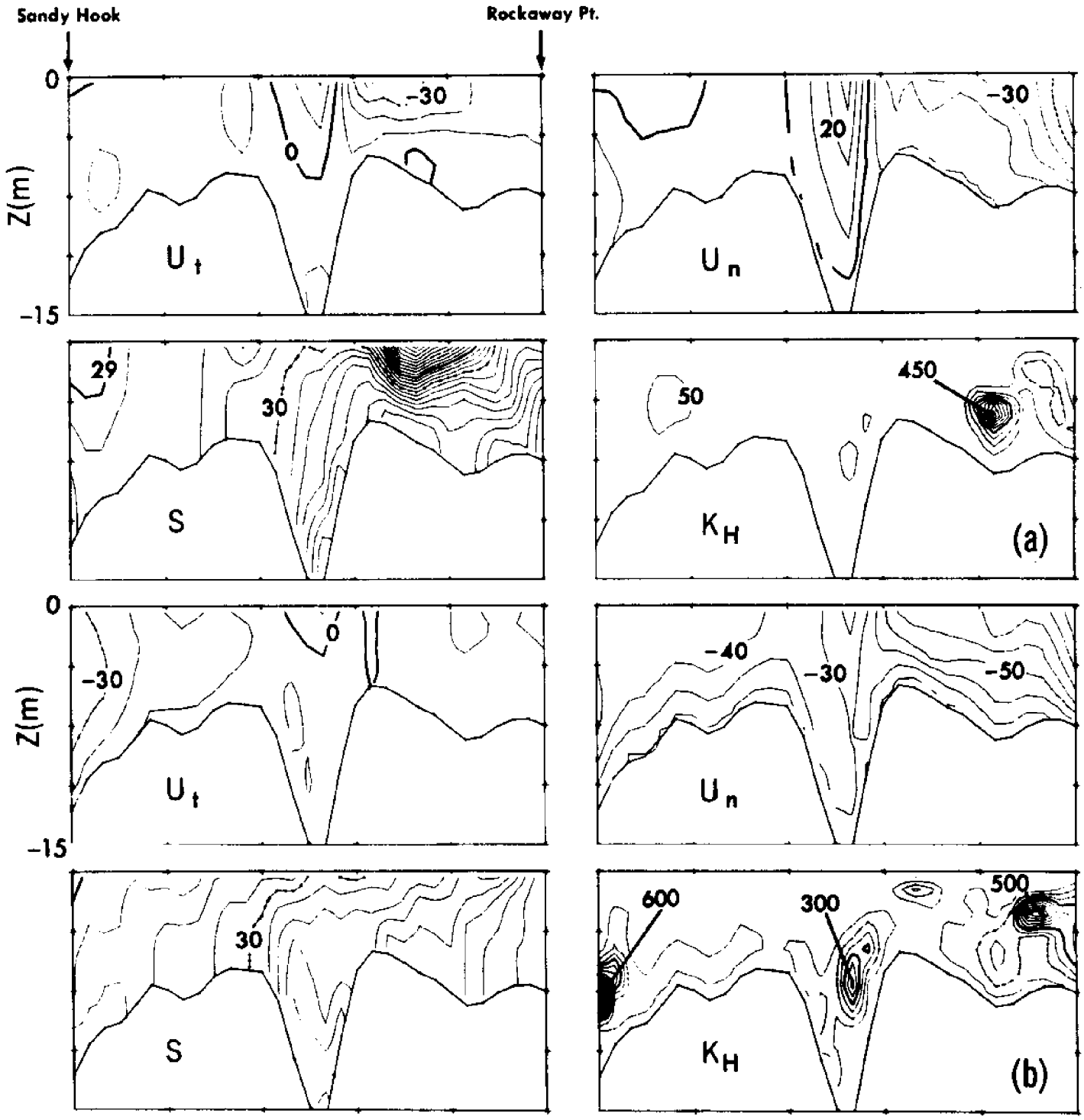


Figure 7a. Computed Contours at 22:00 hours near the beginning of flood, August 19th, 1980, of the velocity $u_T$ (positive to the right) the normal velocity $u_n$ (positive ebbing), both in $cms^{-1}$, the salinity S in ppt and the turbulence mixing coefficient $K_H$ for salt in $cm^2s^{-1}$ at the Sandy Hook-Rockaway Point transect. The heavy dotted line denotes values of 30 $cms^{-1}$ for $u_T$, 50 $cms^{-1}$ for $u_n$, 30 ppt for S and 400 $cm^2s^{-1}$ for $K_H$. The heavy solid line denotes values of 0 $cms^{-1}$ for $u_T$ and $u_n$, 29 ppt for S and 200 $cm^2s^{-1}$ for $K_H$. The light dotted line denotes values of -30 $cms^{-1}$ for $u_T$, -50 $cms^{-1}$ for $u_n$, 28 ppt for S and 100 $cm^2s^{-1}$ for $K_H$. The contour intervals are: 10 $cms^{-1}$ for $u_T$ and $u_n$, 0.25 ppt for S and 50 $cm^2s^{-1}$ for $K_H$.

Figure 7b. Contours at 23:00 hours, August 19th.

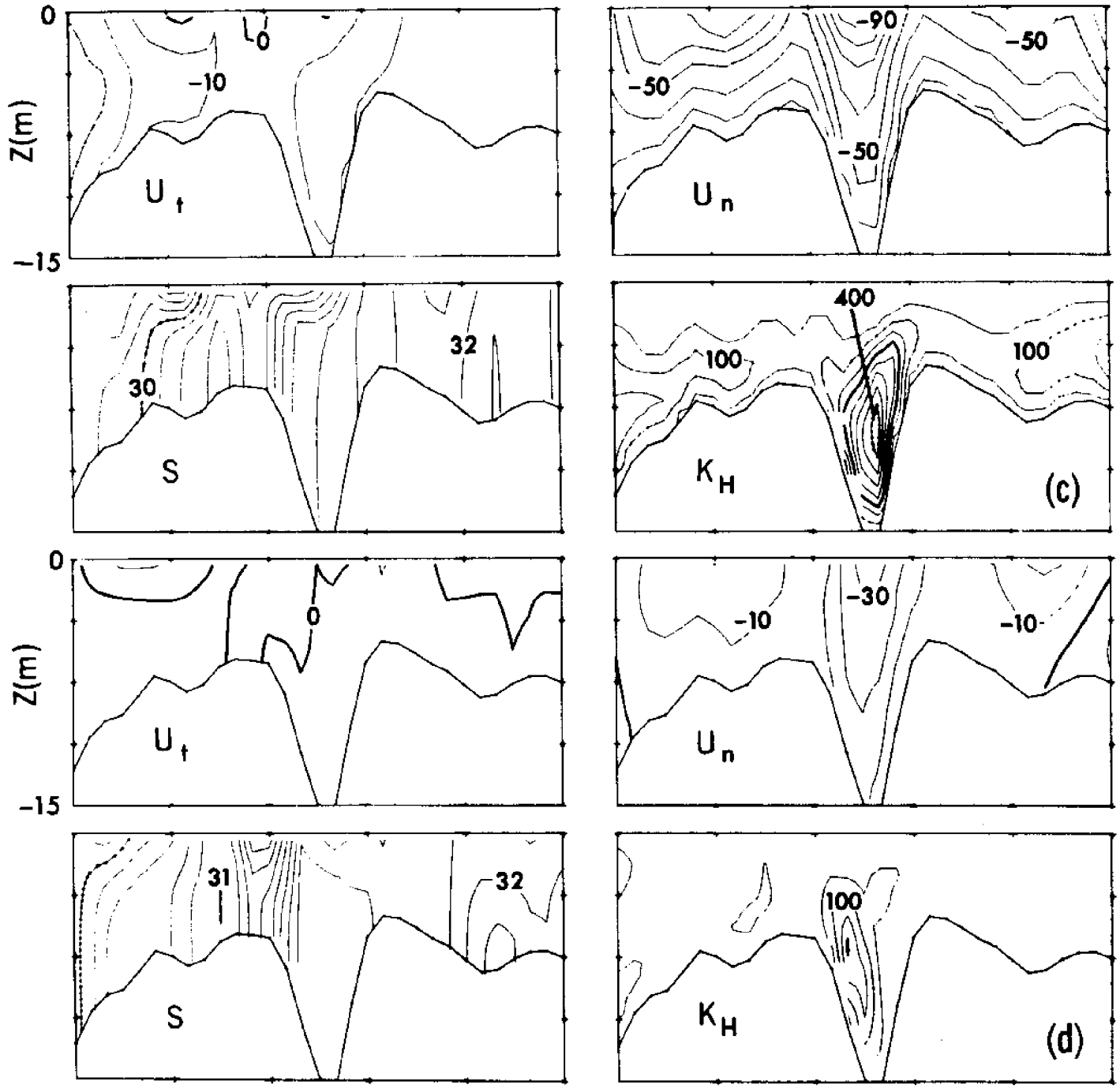


Figure 7c. Contours at 01:00 hour, August 20th.

Figure 7d. Contours at 03:00 hours near the beginning of ebb.

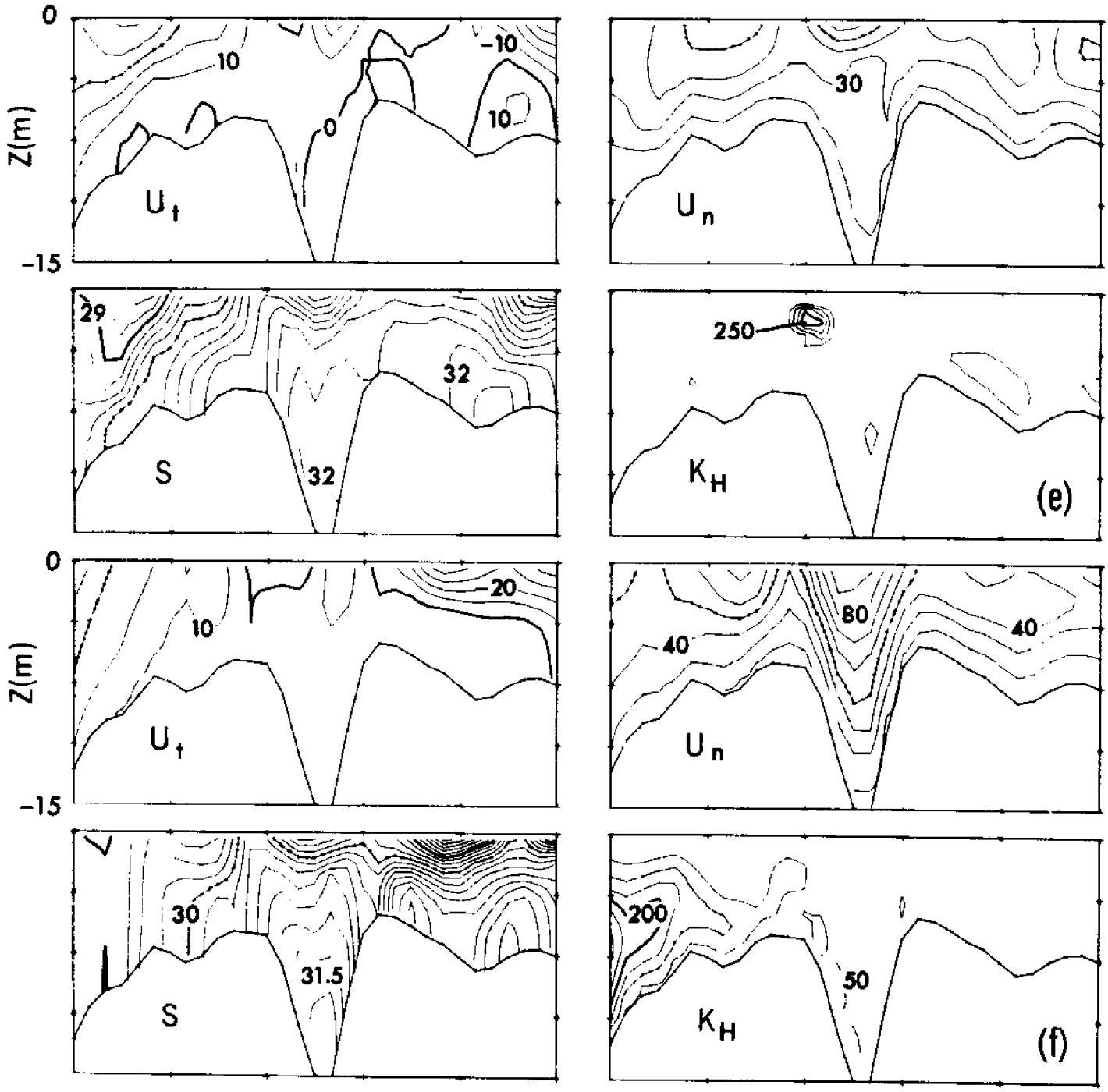


Figure 7e. Contours at 05:00 hours.

Figure 7f. Contours at 07:00 hours.

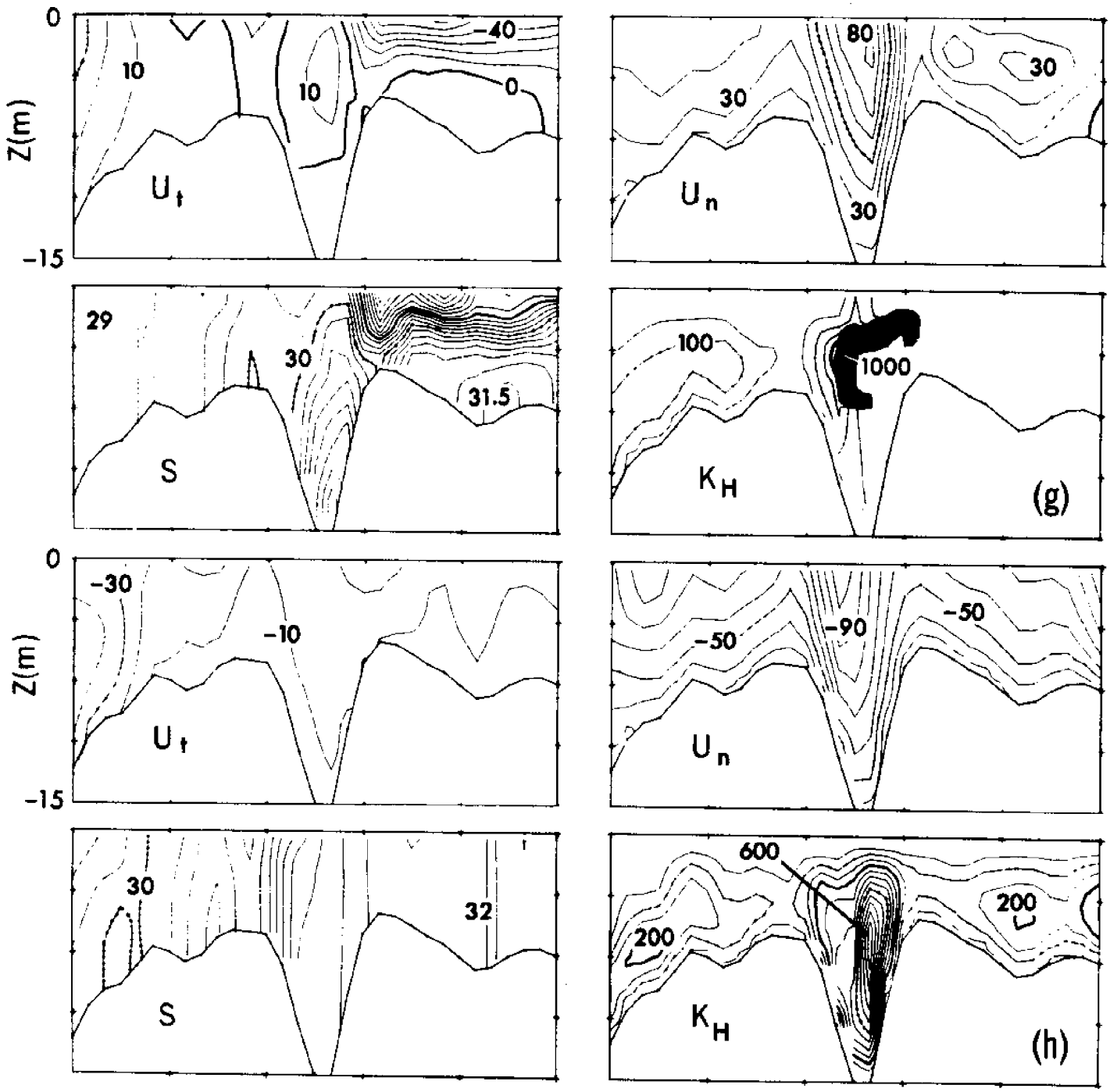


Figure 7g. Contours at 09:00 hours.

Figure 7h. Contours at 13:00 hours.

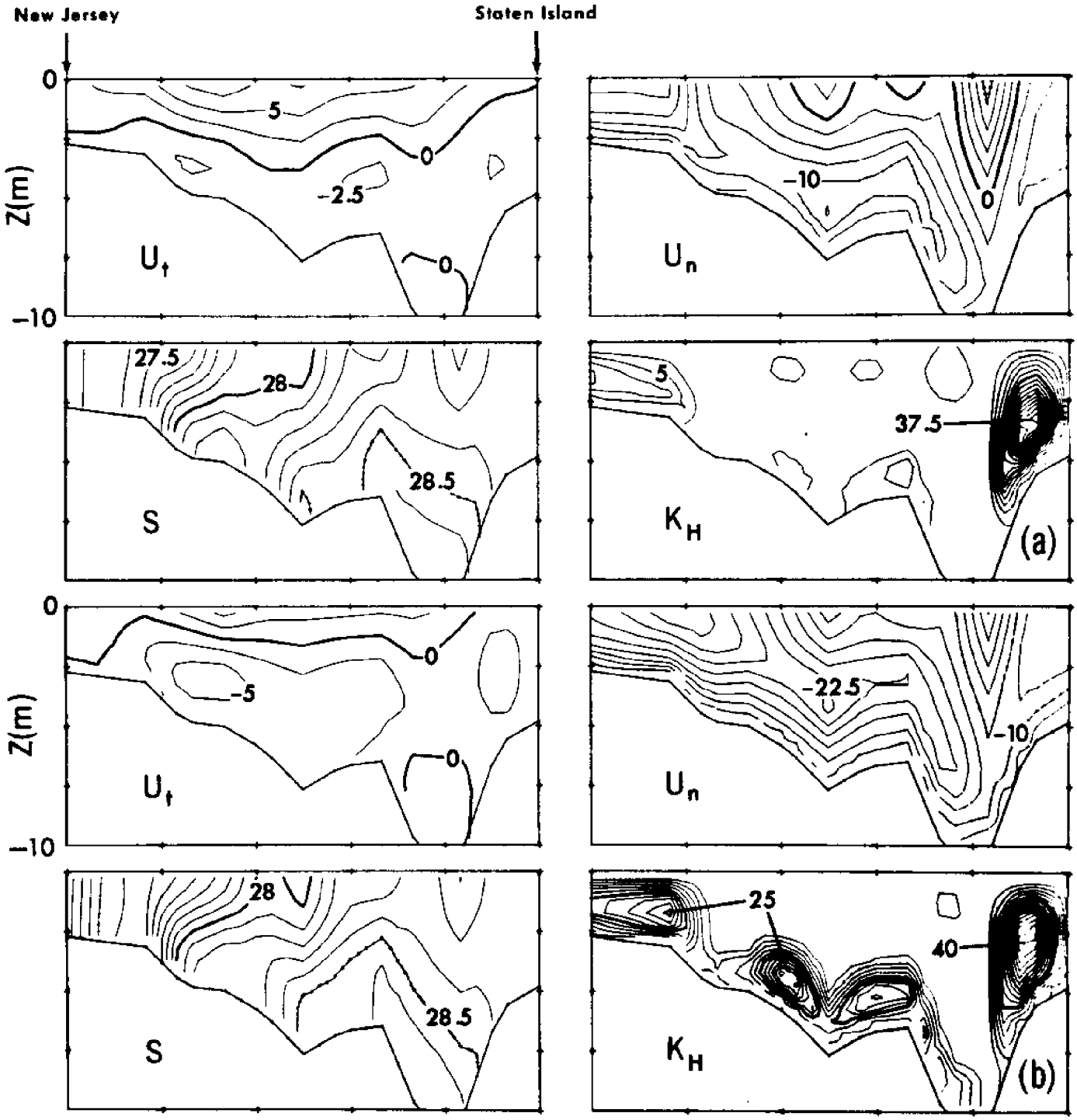


Figure 8 • Caption same as figure 7 but for a section in Raritan Bay. The heavy dotted line denotes values of 10 cms$^{-1}$ for $u_T$ and for $u_n$, 28.5 ppt for S and 25 cm$^2$s$^{-1}$ for $K_H$. The heavy solid line denotes values of 0 cms$^{-1}$ for $u_T$ and $u_n$, 28 ppt for S and 15 cm$^2$s$^{-1}$ for $K_H$. The light dotted line denotes values of -10 cms$^{-1}$ for $u_T$ and for $u_n$, 27.5 ppt for S and 5 cm$^2$s$^{-1}$ for $K_H$. The contour intervals are: 2.5 cms$^{-1}$ for $u_T$ and $u_n$, 0.1 ppt for S and 2.5 cm$^2$s$^{-1}$ for $K_H$.

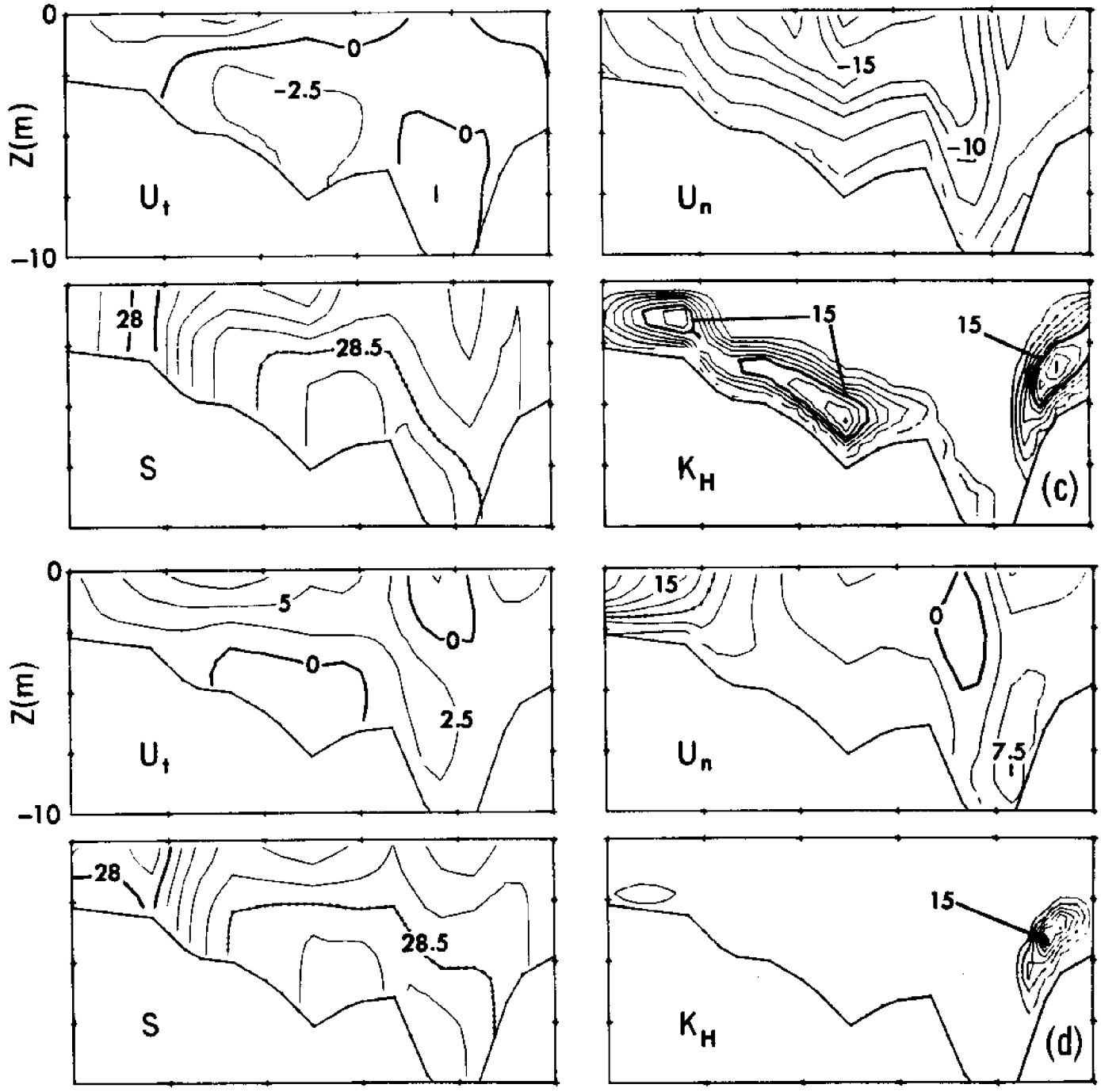
0
Z(m)
-10
0
-2.5
0
$U_t$
-15
-10
$U_n$
28
28.5
S
15
15
$K_H$
(c)
0
Z(m)
-10
5
0
0
2.5
$U_t$
15
0
7.5
$U_n$
28
28.5
S
15
$K_H$
(d)

Figure 8c,d.

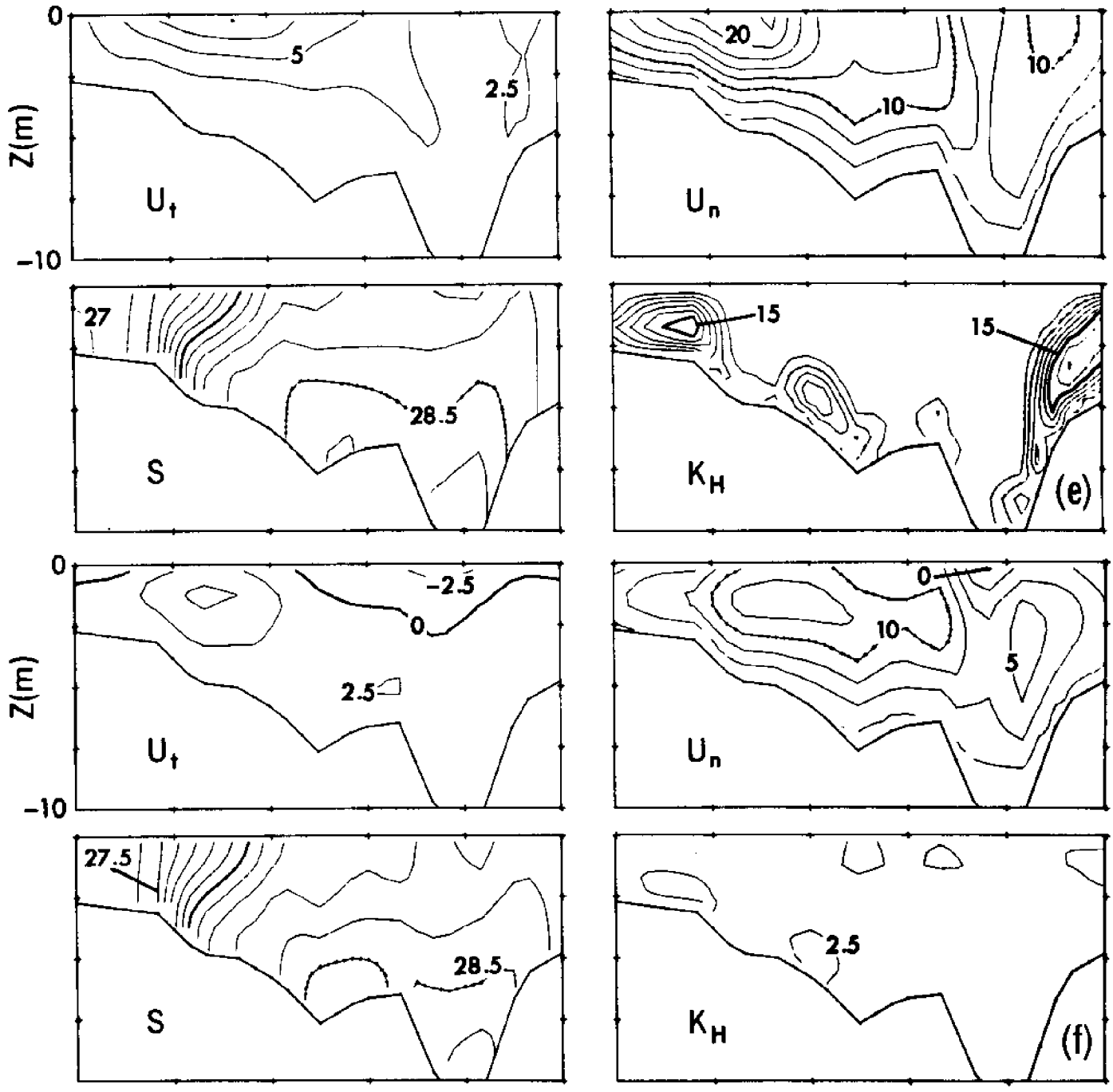
0
Z(m)
-10
5
2.5
$U_t$
20
10
10
$U_n$
27
28.5
S
15
15
$K_H$
(e)
0
Z(m)
-10
-2.5
0
2.5
$U_t$
0
10
5
$U_n$
27.5
28.5
S
2.5
$K_H$
(f)

Figure 8e,f.

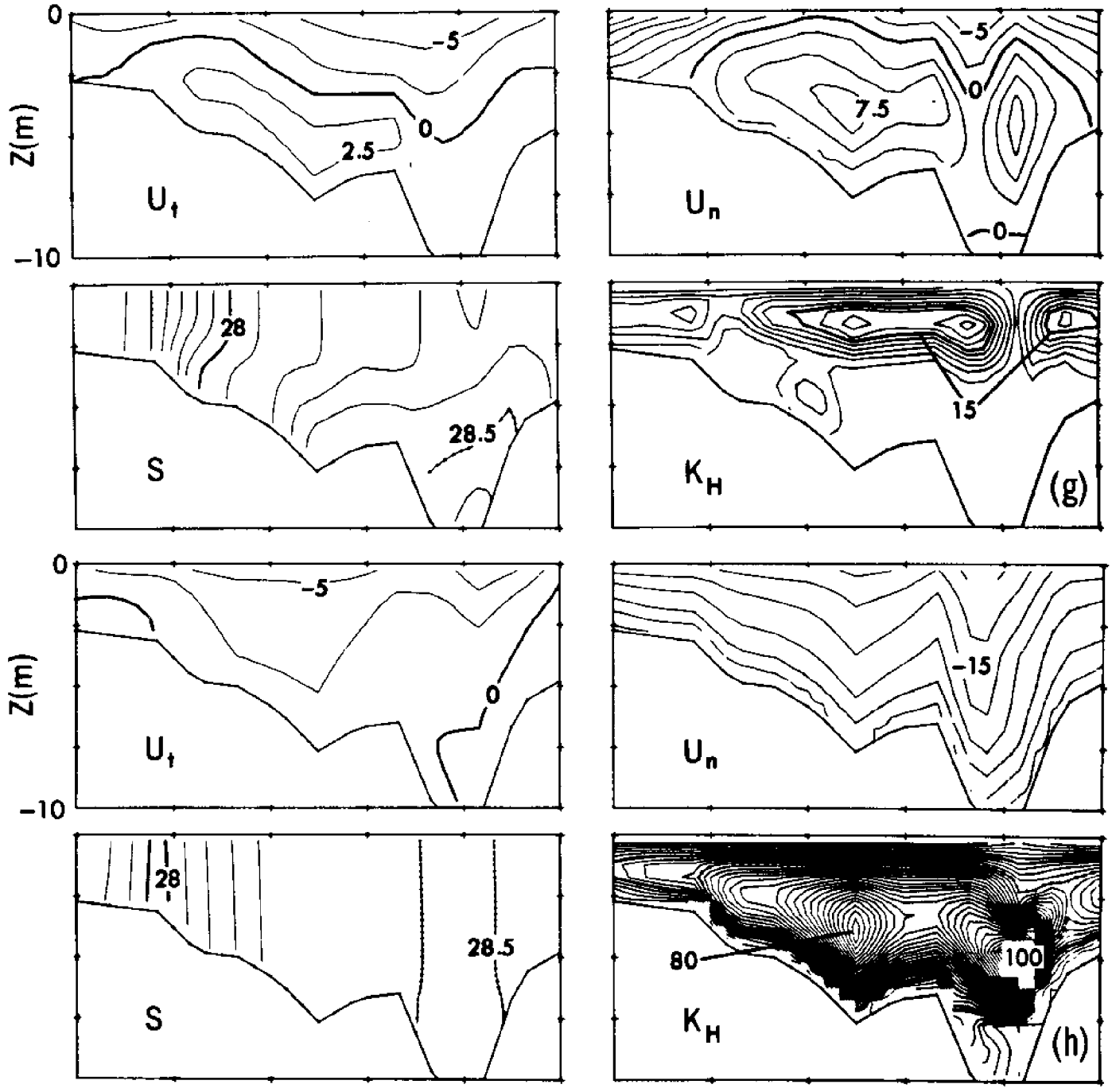
0
Z(m)
-10
-5
0
2.5
$U_t$
-5
0
7.5
$U_n$
0
28
28.5
S
15
$K_H$
(g)
0
Z(m)
-10
-5
0
$U_t$
-15
$U_n$
28
28.5
S
80
100
$K_H$
(h)

Figure 8g,h.

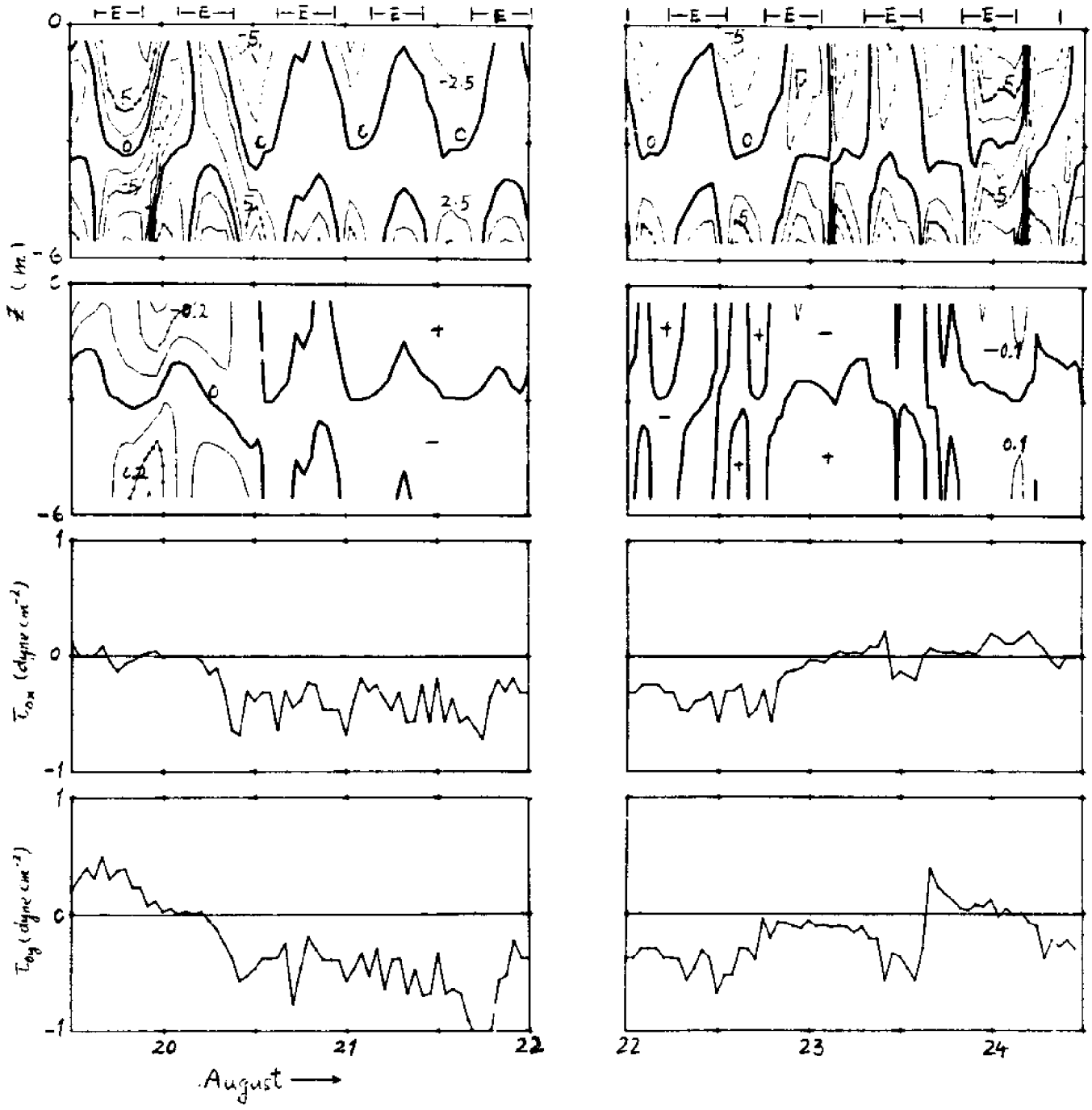


Figure 9 . Time-depth plots of deviations of velocity ($cms^{-1}$, top pannel) and salinity (ppt, second pannel from the top) from their vertical averages in the mid-position of the cross-section in the Raritan bay. The heavy solid contour lines denote zero values of either the velocity or the salinity deviations. Ebbing periods are marked by the letter "E" on the top of the figure. The axial wind stress (third pannel from the top) and the cross-channel wind stress (bottom pannel) in $dynes.cm^{-2}$ are also shown.

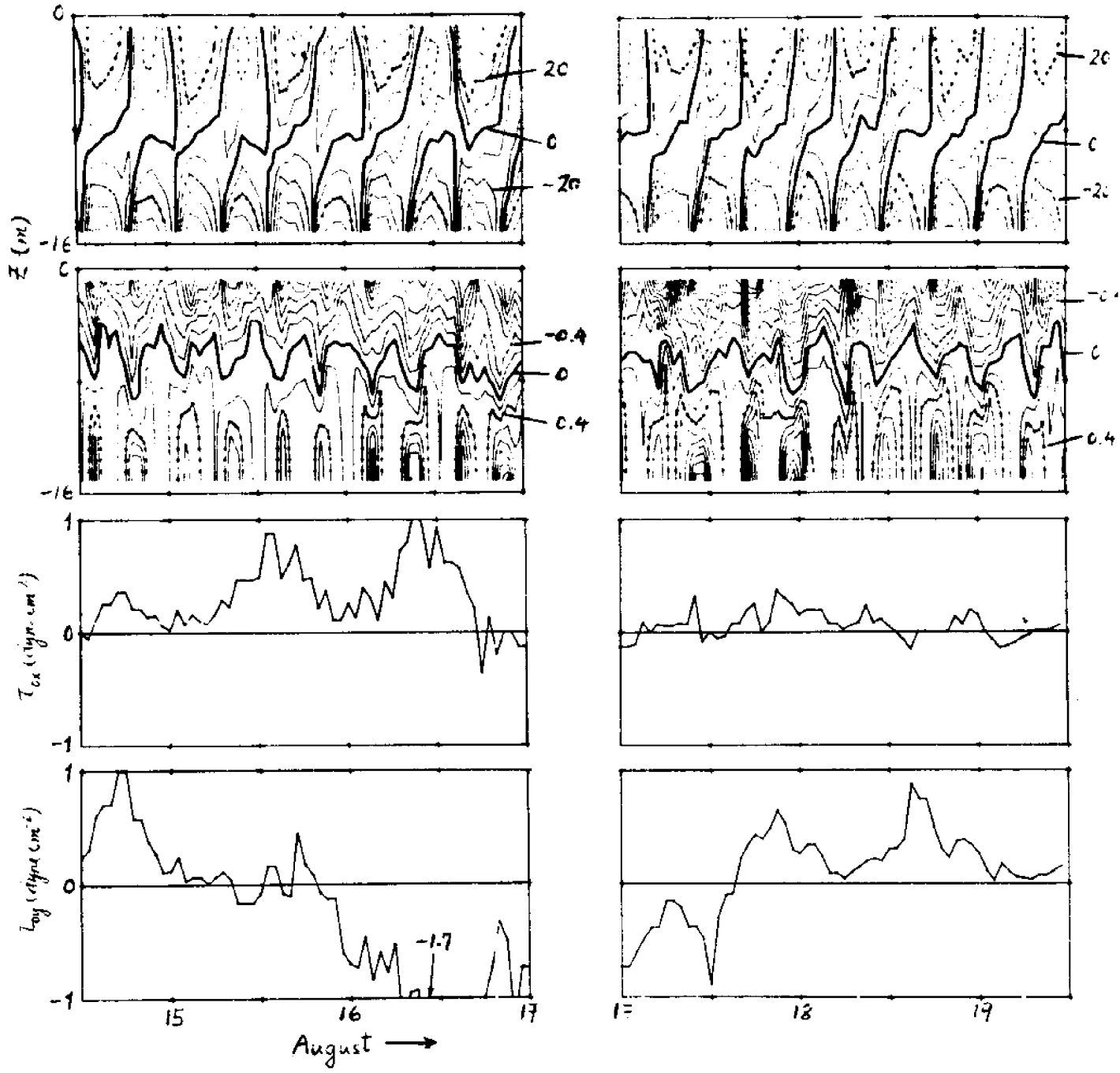


Figure 9b. Same as figure 9a but now at a mid-position of the cross-section in the Narrows covering a different period of up-estuary wind event.

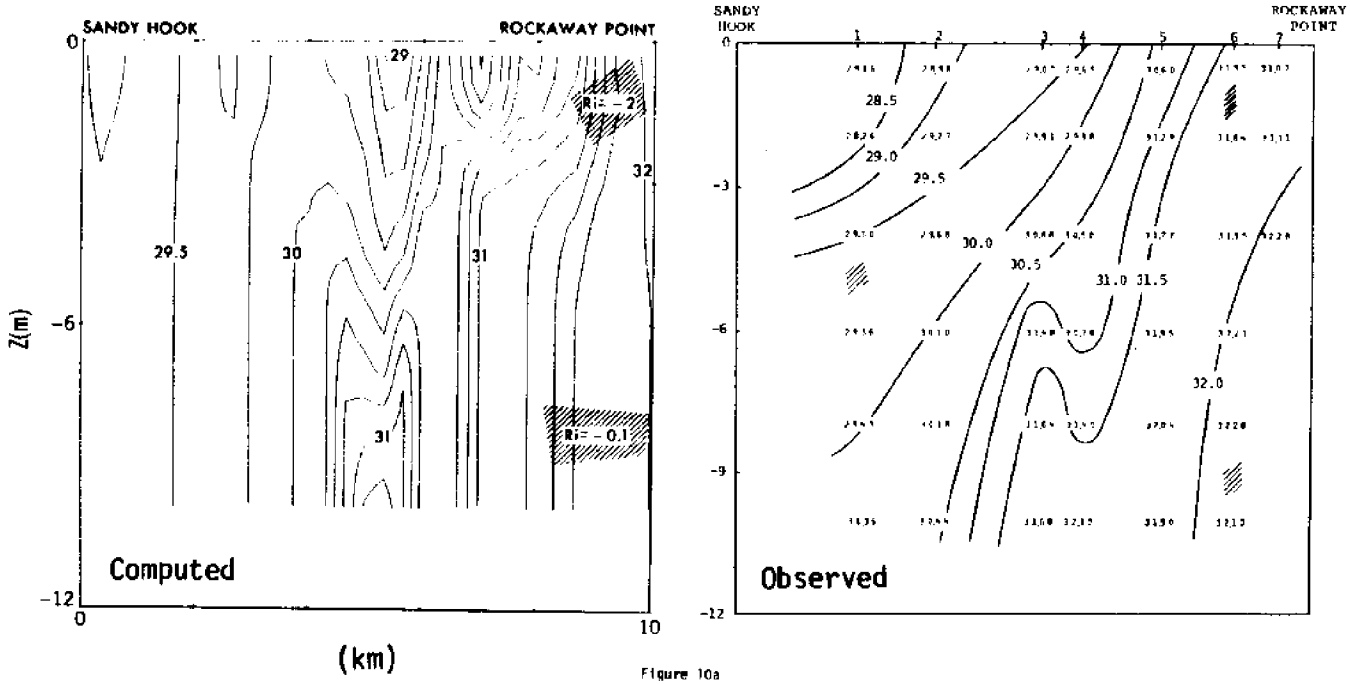


Figure 10a

Figure 10 . Comparison of computed (left panel) and observed salinity distributions across the Sandy Hook-Rockaway transect. The hatched areas are where the water columns are unstably stratified. The computed gradient Richardson numbers Ri are also shown. (a) August 20, 10:00; (b) August 27, 16:00; (c) August 20, 15:00; (d) August 27, 10:00. (a) and (b) correspond approximately to slack before flood and (c) and (d) to slack before ebb.

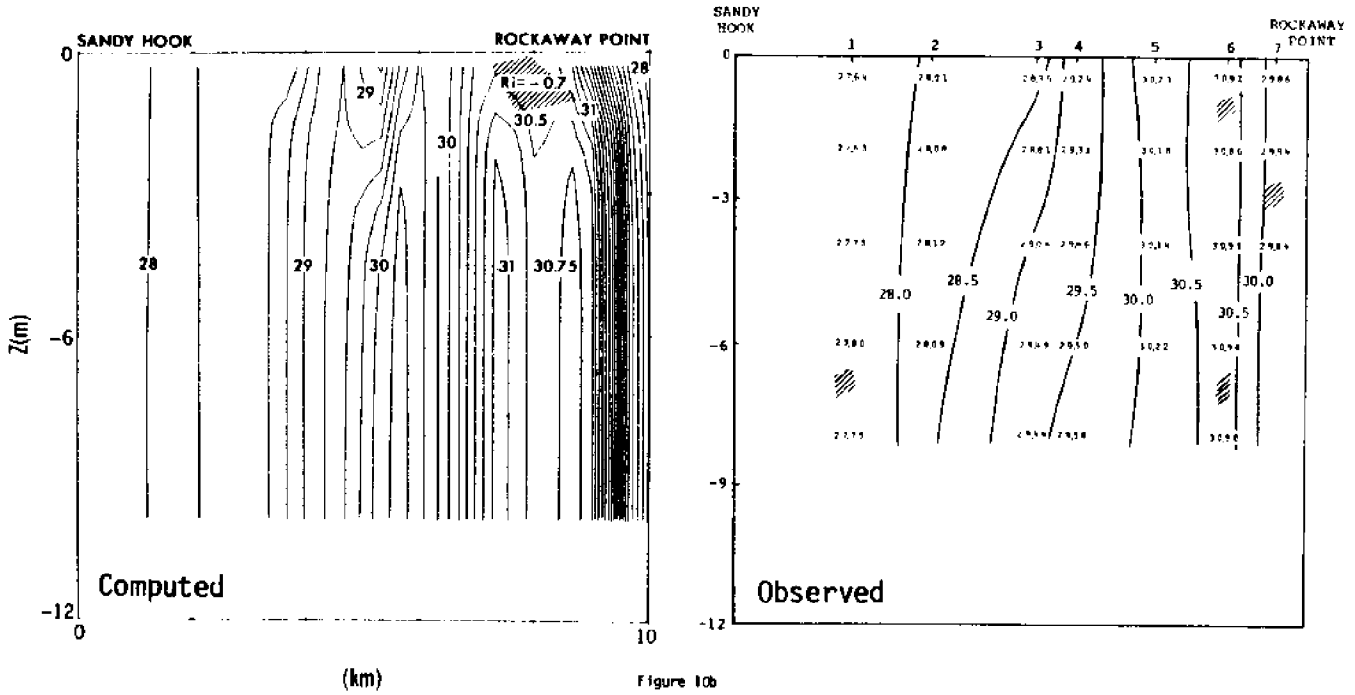


Figure 10b

Figure 10b.

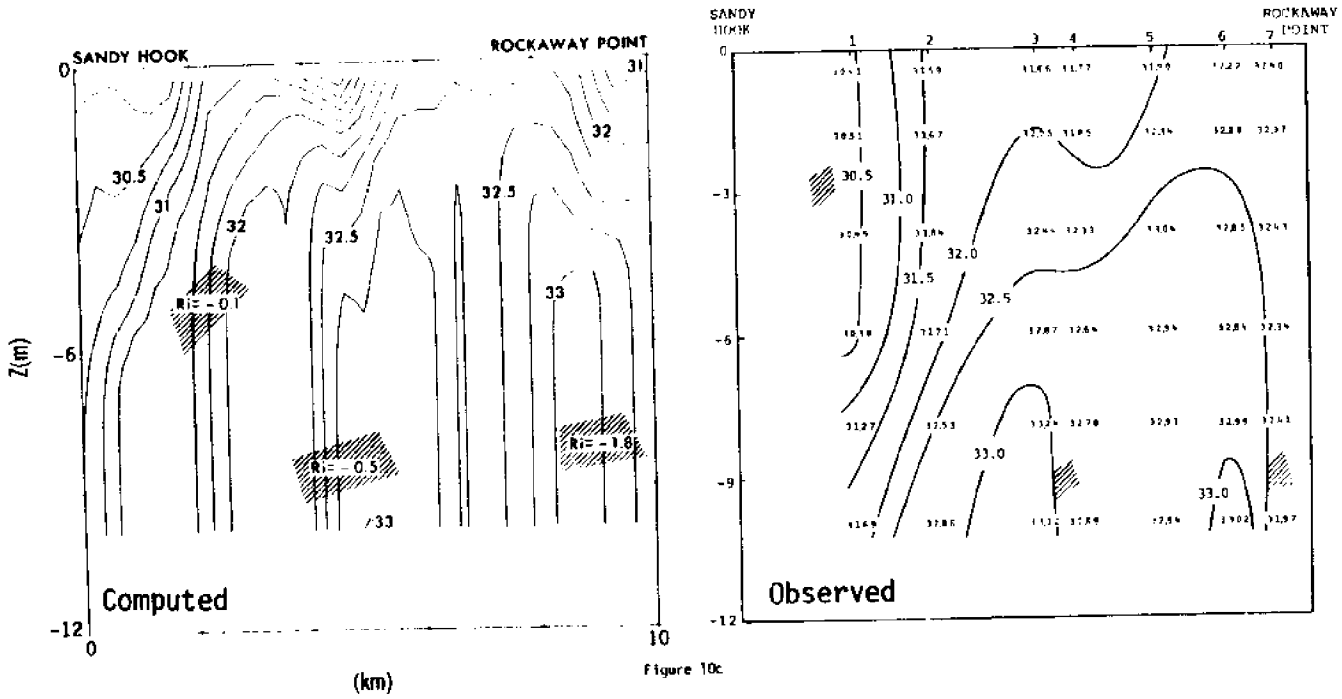


Figure 10c

Figure 10c.

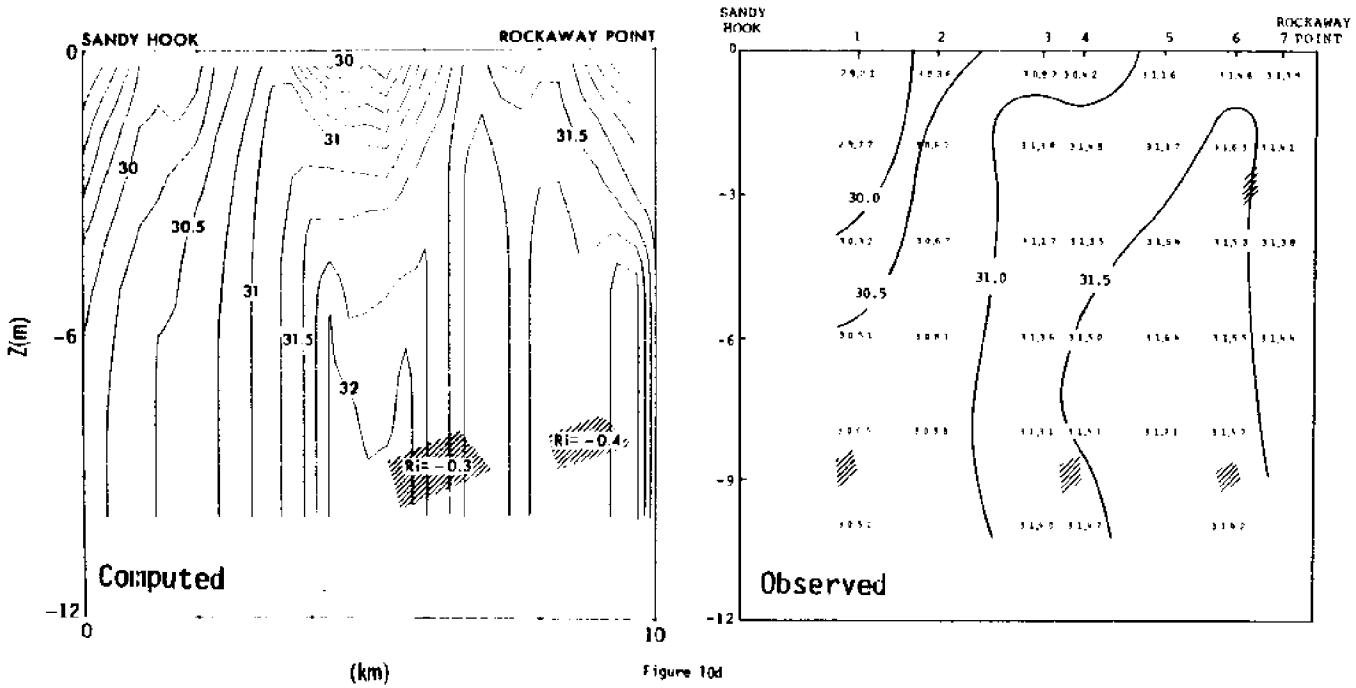


Figure 10d

Figure 10d.

Figure 11a,b

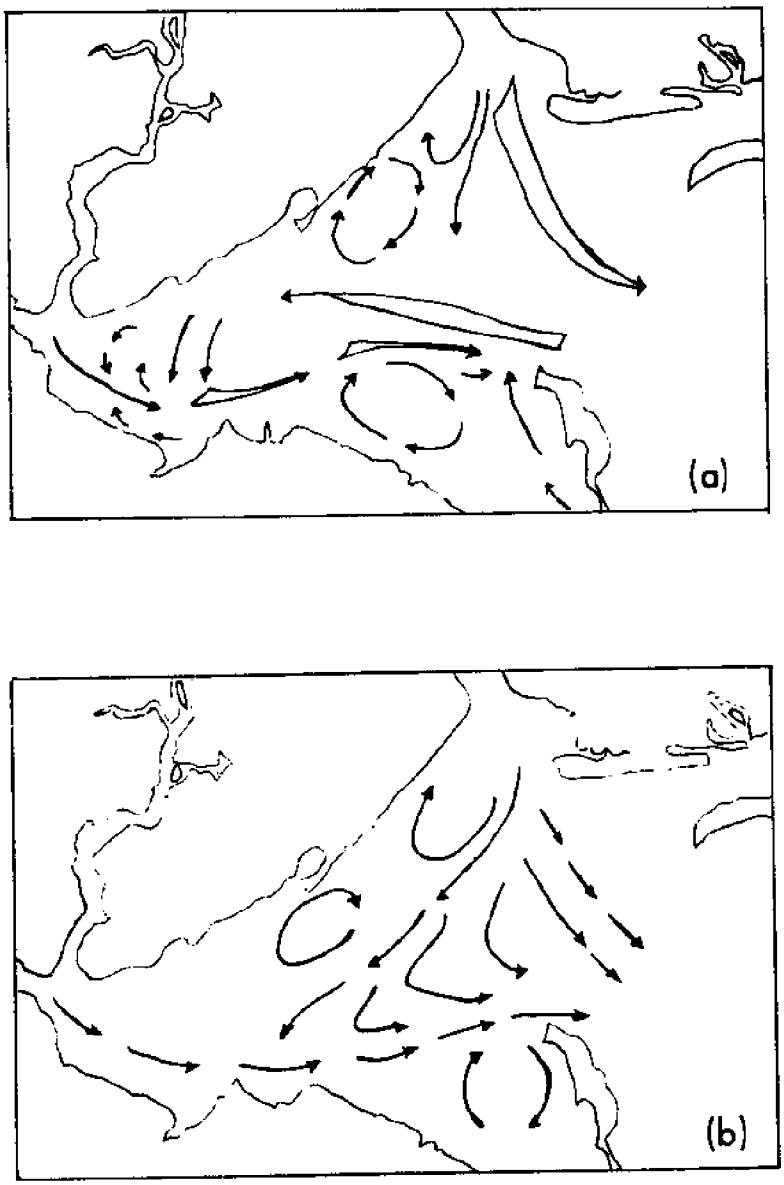


Oey, Figure 11a,b

Figure 11a,b. Near-surface residual circulation in Raritan Bay inferred by (a) Jefferies (1962) and (b) Abood (1972), from accumulated observations made mostly during the Summer season when the wind is predominantly light south-westerly.

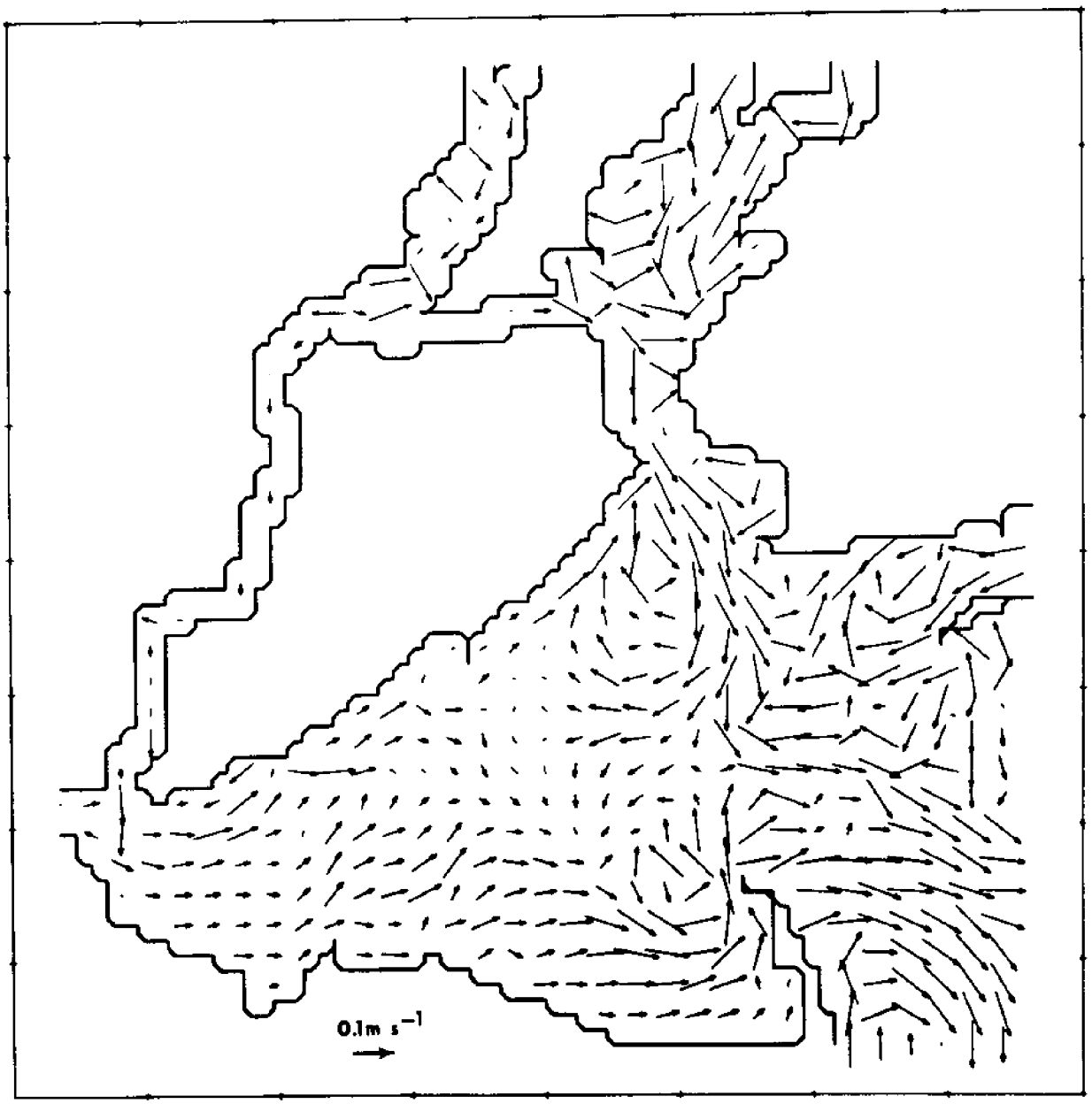


Figure 12. Six days time-averaged computed surface circulation in the estuary. The time average is centered at 00:00 on August 12. The wind during this period is light south-westerly, typical of the Summer wind condition in the estuary.